Characterization and Dating of Argillic Alteration in the Mercur Gold District, Utah

PAULA N. WILSON AND W. T. PARRY

Department of Geology and Geophysics, University of Utah, Salt Lake City, Utah 84112

Abstract

The Mercur gold district of north-central Utah includes several sediment-hosted disseminated gold deposits which are located in the lower member of the Mississippian Great Blue Limestone. Argillic alteration of host limestone consists of illite (R3 illite-smectite <10% S) + kaolinite + quartz ± Fe oxides or pyrite. Argillized limestone has identical clay mineralogy in both oxidized and unoxidized rock. Unlike some other sediment-hosted disseminated gold deposits, variations in the Kubler index and illite/kaolinite ratios show no spatial relationship to faults or to gold distribution within the mineralized areas.

Hydrothermally altered Long Trail Shale, the middle member of the Great Blue Limestone, also occurs within the Mercur district and surrounding region. The shale varies in mineralogy from an assemblage consisting of R1-type illite-smectite (20–35% smectite) + chlorite + kaolinite + quartz + pyrite or Fe oxides to an assemblage consisting of R3-type illite-smectite (5–10% smectite) + kaolinite + quartz + pyrite or Fe oxides. Shale with R3 illite-smectite is most highly altered and is mineralogically and chemically very similar to the highly altered limestone within the gold deposits. Both the altered shale and the altered limestone contain veins of R3 illite-smectite + kaolinite ± quartz and pyrite or Fe oxides. Additional hydrothermal features exhibited by both shale and limestone are felted and interlocking clay mineral textures, radiating clay mineral habits, crosscutting and replacement clay mineral textures, and fossil replacement by clay minerals and quartz.

Ten K-Ar ages of illite-rich clay-size separates of argillically altered and mineralized limestone from the Mercur deposits range from 98.4 to 226 Ma. None of the hydrothermal illites in the deposit have Tertiary ages. These ages are similar to a range of Mesozoic ages previously obtained for vein and matrix clay in the Long Trail Shale. Most of these ages are interpreted as mixed ages resulting from overprinted thermal and/ or mass transfer events. Completely argillized and highly mineralized limestone obtained from the Carrie Steele fault yields an age of 152 ± 4 Ma (0.03–0.3-μm-size fraction) that is interpreted as the best estimate of the age of the gold-bearing hydrothermal event on this fault. The age data, the widespread mineralization, and the expected thermal influence of the Tertiary Eagle Hill Rhyolite calculated using published models indicate that gold deposition at Mercur is not related to Tertiary igneous activity. The complex thermal history of these deposits prevents a precise determination of the age of gold deposition. Comparison of age data from the Mercur deposits and the Long Trail Shale suggest gold mineralization may have occurred between 140 and 160 Ma.

Introduction

A WIDE range of low- to moderate-temperature geologic processes can be identified and characterized in altered sedimentary rocks. These processes include diagenesis, burial metamorphism, fluid flow in basins, low-grade metamorphism related to thrust belt formation, contact metamorphism, and mineral deposit genesis. Characterization and chronology of these types of events are crucial to understanding the genesis of sediment-hosted disseminated gold deposits. Because these processes occur at relatively low temperatures, clay petrology and K-Ar dating of clay minerals have been the most widely used techniques for their characterization. Illite-group minerals in particular are the key to these methods for three reasons: they commonly occur in sedimentary rocks, their variation in smectite content and ordering type record the effects of low- to moderate-temperature events (Srodon, 1984; Srodon and Eberl, 1984), and they are suitable for K-Ar dating (Aronson and Lee, 1986; Hunziker et al., 1986).

Dating of sediment-hosted disseminated gold deposits has proven difficult because the paragenesis of the submicron gold is difficult to discern, they lack mineralized veins bearing a datable mineral, and well-defined crosscutting relationships with other datable geologic events in the deposits are rare. This leaves the dating of hydrothermal illite as the most reli-

able technique for dating alteration, and by inference, mineralization (Clauer and Chaudhuri, 1992; Clauer et al., 1992). However, a major problem with low- to moderate-temperature events in sedimentary rocks is that they may not be of high enough temperature and/or long enough duration to reset completely the K-Ar ages of previously existing minerals. As a result, radiometric age studies often produce a data cloud consisting of mixed ages that can be difficult to interpret in terms of the ages of end-member components. Dating of alteration at sediment-hosted disseminated gold deposits using illite has previously been attempted by us on shales in the Mercur district (Wilson and Parry, 1990a) and by Arehart et al. (1993) at the Post-Betze deposit in the Carlin trend, Nevada. Both studies revealed a range of dates, which represents possible mixing between illites of detrital, diagenetic, hydrothermal, or reset detrital and diagenetic origins. Although neither study obtained well-defined age estimates for the deposits investigated, they both provided evidence suggesting that gold deposition was older than had been previously assumed.

The purpose of this paper is twofold. First, we describe the clay mineralogy of argillically altered limestone from within the Mercur gold deposits and compare it to the regional shale alteration mineralogy. Second, we present new illite K-Ar data from within the Mercur deposits. Data pre-
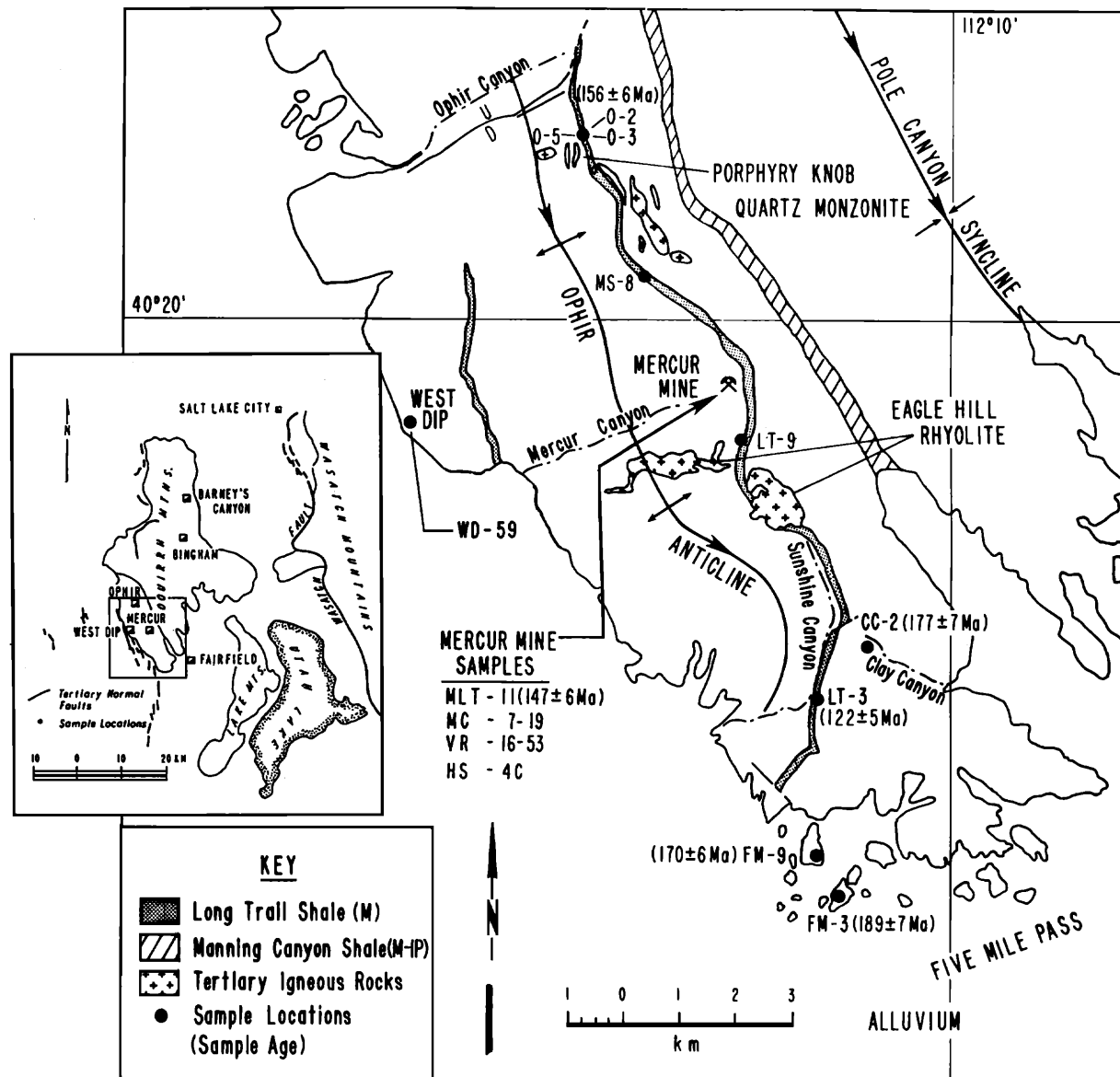
1197

FIG. 1.   General geology of the southern Oquirrh Mountains showing sample locations (after Gilluly, 1932). K-Ar ages are shown for vein samples. Insert is a regional map showing the location of the study area.

sented here document a complex thermal history for the Mercur district that is still not well understood. The data do show that extensive argillic alteration of limestone within the Mercur gold deposits is related to districtwide argillic alteration that is Mesozoic in age. Hydrothermal activity on a highly mineralized fault is postulated as occurring at near 150 Ma. Subsequent hydrothermal effects by the Tertiary Eagle Hill Rhyolite had no significant role in either the gold mineralization or the argillic alteration.

Geology of the Mercur District

The Mercur district is located in the southern Oquirrh Mountains of north-central Utah and is 90 km southwest of Salt Lake City (Fig. 1). The district extends from Ophir Canyon south to Five Mile Pass. The sedimentary rock column

consists of a 7.5-km-thick sequence of late Paleozoic sediments that were deposited in the Oquirrh basin, a northwest-trending structural basin (Jordan and Douglass, 1980). Two separate compressional tectonic events are evident: a Jurassic event (Wilson, 1992; Presnell and Parry, in press) and the Late Cretaceous to Early Tertiary Sevier orogeny (Armstrong, 1968).

The gold deposits of the Mercur district occur in a carbonate sequence of upper Paleozoic sediments that have been deformed into a series of large amplitude northeast-trending folds (Gilluly, 1932; Kornze, 1987). These folds are interpreted as ramp folds over a thrust fault (Kroko, 1992; Presnell et al., 1993; Presnell and Parry, in press). The gold deposits of the Mercur district occur at Mercur, Sunshine Canyon, West Dip, the south side of Ophir Canyon, and between

OQUIRRH FORMATION

MANNING CANYON
FORMATION

GREAT BLUE
FORMATION

Upper Member

Long Trail Shale
Member

Lower Member

Mercur Mine Series

Upper Beds

Mercur Beds

Barren Beds

Magazine Sandstone
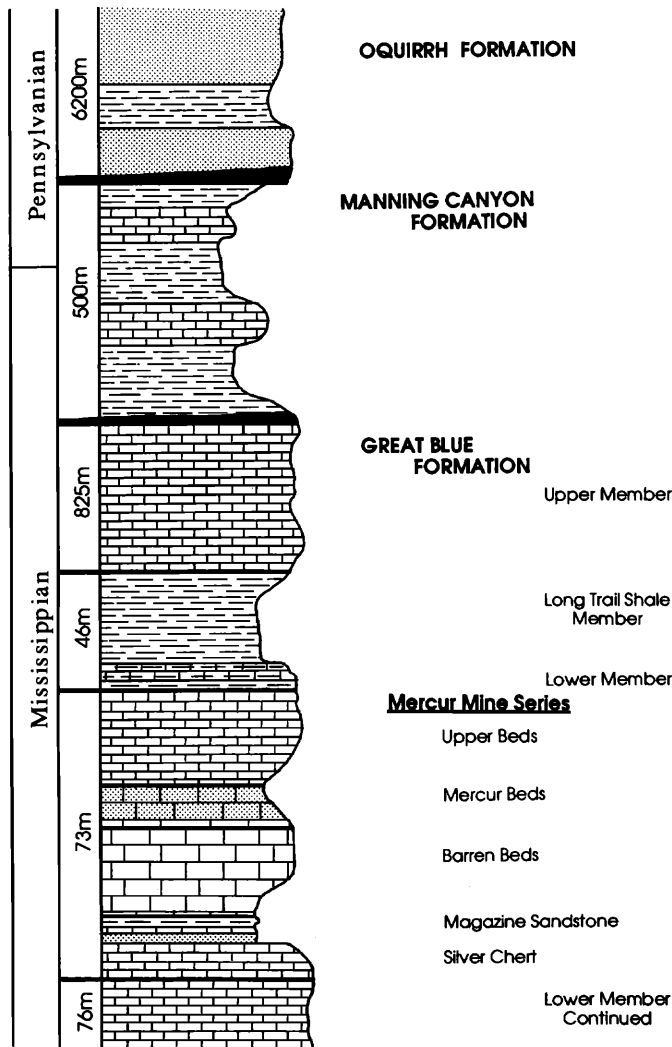
Silver Chert

Lower Member
Continued

FIG. 2. Schematic stratigraphic column of upper Paleozoic sediments in the study area. Names for the various units of the lower mineralized member of the Great Blue Formation, known as the Mercur Mine Series, are also shown.

Ophir Canyon and Mercur (Fig. 1). The deposits occur along the east and west limbs of the Ophir anticline. High-angle faults, which resulted from tensional flexure during the formation of the anticline, control the gold mineralization (Kroko, 1992).

The gold deposits occur in a mineralized sequence of the lower member of the Mississippian Great Blue Limestone locally known as the Mercur mine series (Fig. 2). The middle member of the Great Blue Limestone, the Long Trail Shale, is also weakly mineralized (Gilluly, 1932; Wilson and Parry, 1989, 1990b). A second shale, the Mississippian-Pennsylvanian Manning Canyon Shale, lies above the Great Blue Limestone. Both the Long Trail and Manning Canyon Shales have been extensively hydrothermally altered throughout the southern Oquirrh Mountains, although the Manning Canyon Shale does not contain gold (Wilson and Parry, 1990a; Wilson, 1992).

Two Tertiary igneous intrusions are present in the Mercur

district (Fig. 1). The 37 Ma Porphyry Knob quartz monzonite includes several small outcrops which total 0.2 km^2 and are located 3.0 km north of the Mercur mine. The 31.5 Ma Eagle Hill Rhyolite (Moore and McKee, 1983) occurs within the most highly mineralized portion of the district. It has a total outcrop area of 0.4 km^2 and is generally a dike. The rhyolite is a microcrystalline and equigranular assemblage of sanidine and quartz. In the Sacramento pit the rhyolite has a chilled margin that is cryptocrystalline to glassy. The rhyolite is locally altered with feldspars converted to clay minerals.

Gilluly (1932) proposed that the gold mineralization was related to the intrusion of the Eagle Hill Rhyolite. Subsequent work by Tafuri (1987), Kornze (1987), and Jewell and Parry (1987, 1988) recognized the Mercur deposits as sediment-hosted disseminated gold deposits similar to those at Carlin, Nevada. These workers also assumed that the gold mineralization was related to intrusion of the Eagle Hill Rhyolite.

Methods

Sample locations

Material from the Mercur mine was obtained from the Marion Hill, Mercur, and Sacramento pits (Fig. 3). Gold values in the Marion Hill pit are highest along northeast- and smaller northwest-striking high-angle faults, in zones of argillic alteration, and in bedding plane faults (Kroko, 1992). Samples were obtained from limestone of the Upper beds on the east side of the pit, known as the Brickyard area, where the Carrie Steele fault is a grabenlike structure (Fig. 4). The graben is about 65 m wide in this area and trends N 30°–40° E.
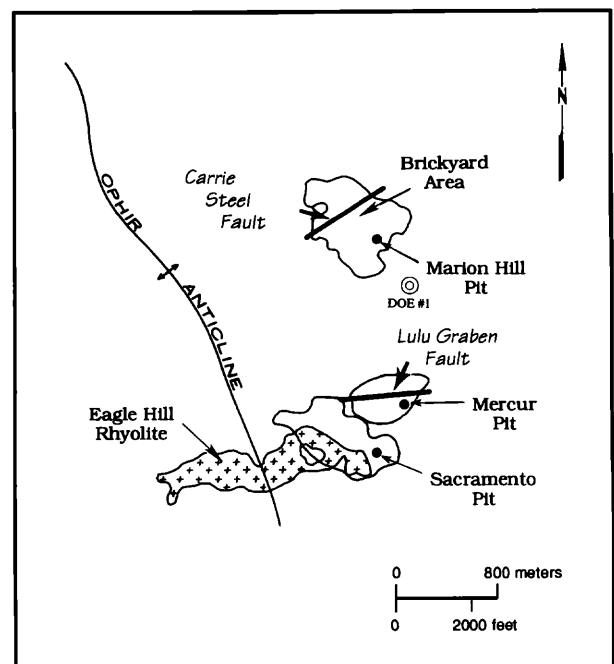

FIG. 3. Map of the Mercur mine area showing locations of the open pits and the Eagle Hill Rhyolite. The positions of the Carrie Steele and Lulu Graben faults are schematic. The open circle shows the location of the deep drill hole DOE #1.
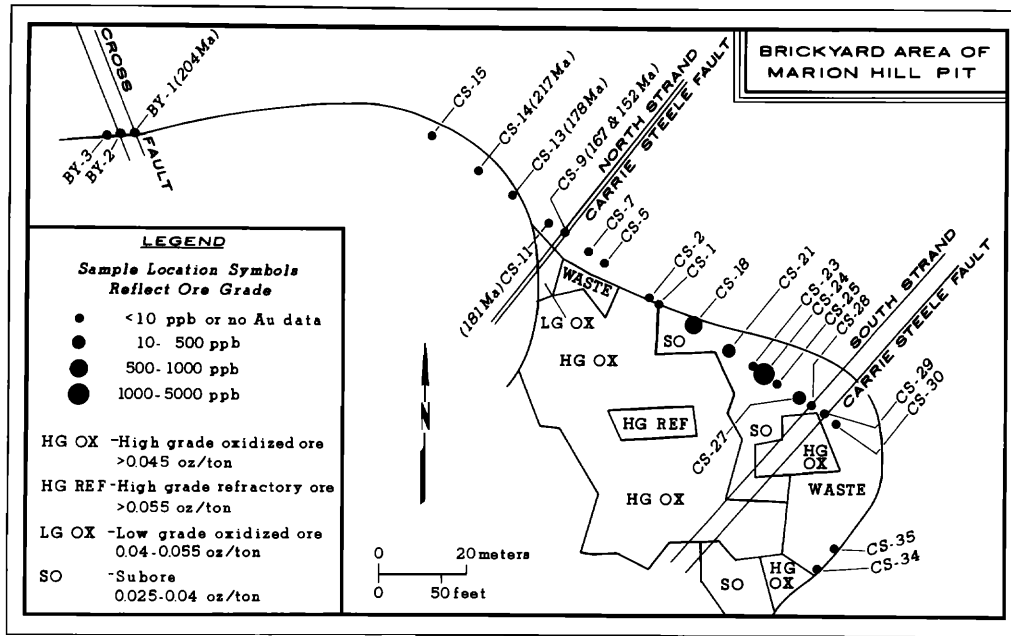
FIG. 4. Sample location map for the 6,770 ft level in the upper bed limestones of the Brickyard area of the Marion Hill pit. Fault zones are shown as double parallel lines. Sample locations are shown by solid circles whose size is keyed to gold content. Ages of dated samples are also shown. Types and grades of ore in the unmined portion of the level at the time of sample collection are indicated.

The Mercur pit lies to the south of the Marion Hill pit (Fig. 3). Gold distribution is controlled by the east-northeast striking Lulu graben structure and the north-south-trending Twist fault zone (Stanger, 1990). Samples were obtained in the interior of the pit from the Mercur beds and the Magazine sandstone (Figs. 5 and 6).

The Sacramento pit lies farthest to the south, adjacent to and partially within the Eagle Hill Rhyolite (Fig. 3). Although there are a few areas of intense argillization, the rhyolite is generally only weakly altered and contains gold only where it has assimilated country rock (Kroko, 1992; mine personnel, pers. commun.). Samples were obtained in a traverse from the contact of the rhyolite out into surrounding altered limestone.

The clay mineralogy was determined by X-ray diffraction analysis. Oriented smears of various size fractions were ana-
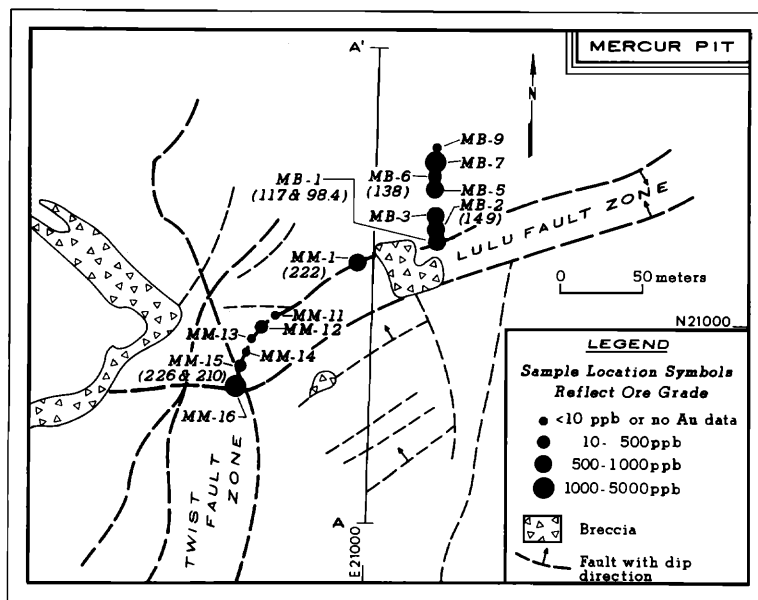

FIG. 5. Simplified geologic map of the Lulu fault zone in the Mercur pit. Sample locations are shown by solid circles whose size is keyed to gold content (after Stanger, 1990).
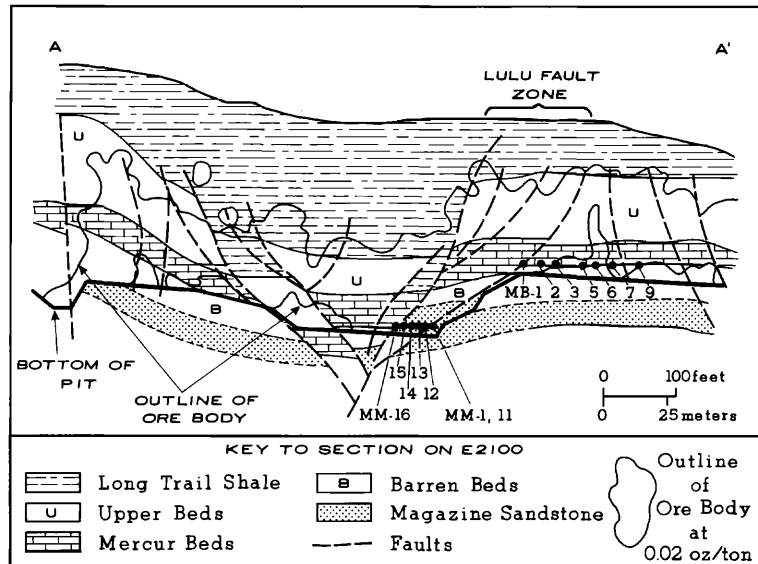
FIG. 6. Cross section on A-A' (see Fig. 5) along section on E21000 showing graben structure of the Lulu fault zone and sample locations in the Mercur beds (MB) and the Magazine sandstone (MM) (modified from Stanger, 1990). These sample locations are projected onto the E 21000 section to show relationships to the structure and stratigraphy. Figure 5 should be consulted for exact locations in relation to this section. The outline of the orebody is shown as a heavy line that is coincident with the bottom of the pit.

lyzed on a Phillips XRG-2600 X-ray diffractometer (Cu Kα). Samples were analyzed from 2° to 45° 2θ using a 1° slit and run speeds of 1°/min. Oriented smears were made using minimal grinding and were peptized by hand stirring or by minimal processing in a blender with deionized water containing 1 to 2 ml of a 5 percent Calgon solution per 100 ml of suspension. Size separates of <2 and 0.03 to 0.3 μm used for mineralogy (XRD) and K-Ar age determination were made using a high-speed centrifuge. Three XRD runs were made on each sample: air dried, glycolated 24 h at 60°C, and heated 1 h at 550°C. The X-ray diffractometer was calibrated using quartz and cholesterol standards.

Three techniques were used to measure the particle size in dated illite samples: conventional pipette analysis (Lewis, 1984), the Scherrer equation (Klug and Alexander, 1974), and photon correlation spectroscopy (PCS; Ford, 1985; Stock and Ray, 1985; Weiner and Tscharnuter, 1987; Lebron et al., 1993).

Illite mineralogy

Interstratified illite-smectite (or illite-smectite minerals; Srodon and Eberl, 1984) consist of various combinations of illite layers (I) and smectite layers (S) stacked parallel to the c axis. When the smectite layers are numerous (>50%) and the stacking sequence is in random order, the material is called R0. When the smectite content is 25 to 50 percent and the stacking sequence has statistical ordering, based on repetition of units consisting of illite-smectite, the material is called R1. When the smectite content is <25 percent, the illitic material is highly ordered and based on repetition of units consisting of illite-smectite-illite-illite, the illite is referred to as R ≥ 3. We will refer to this type of illite simply as R3.

The type of interstratified illite-smectite mineral (i.e., R1

or R3), the amount of smectite in the illite-smectite minerals, and the percentages of each clay mineral found within the clay assemblages were determined by modeling X-ray diffraction data using the computer program NEWMOD (Reynolds, 1985). NEWMOD calculations were made by varying the parameters of percent illite layers, percent potassium in illite layers, illite and smectite (001) spacing, number of layers in the crystallite (n), and type of ordering (R0, R1, R3) until the best match in both peak position and peak height was achieved between the actual and simulated XRD patterns. The estimated error in the percent smectite within the interstratifications is ± 4 percent. The relative proportions of each clay mineral in the dated mineral mixtures were estimated by first modeling each individual clay mineral (kaolinite, pyrophyllite, R1 illite, and R3 illite) with NEWMOD and then numerically mixing them in suitable proportions to obtain the best match with the peak heights and positions on the measured XRD profile in the range of 2° to 27° 2θ.

Kubler index determinations were made on the <2-μm-size fraction material (Kubler, 1967). This index is the width of the (001) illite-smectite peak taken at one-half the peak height measured on a glycolated sample. A Kubler index of 0.25 corresponds to 0 percent smectite in the illite and little variation in particle thickness within the sample. Values between 0.25 and 0.42 correspond to the highest grade of low-grade metamorphism (anchimetamorphic zone) and are also typical of hydrothermal illites. Kubler index values from 0.42 to 0.60 correspond to a higher smectite content and considerable particle size variation which is typical of the highest grade of diagenesis (Kisch, 1991).

Variations in illite-smectite mineralogy are graphically shown on a Watanabe diagram (Watanabe, 1981; Inoue and Utada, 1983; Srodon and Eberl, 1984), which is a plot of the difference in degrees 2θ between the positions of the (001)

TABLE 1.   Argillic Alteration Mineralogy of Sedimentary Rocks Hosting Ore at Mercur

Sample	I-S ordering	Minimum % smectite	Other minerals	Kubler index (°2θ)	Illite/kaolinite ratio (wt %)
Marion Hill pit upper beds					
CS-1 white <2 μm	R3	5	Kao, minor qtz	0.53	49.0
CS-1 black <2 μm	R3	5	Kao, minor qtz	0.55	
CS-2 yellow <2 μm	R3	4	Kao, minor qtz	0.35	2.3
CS-2 black <2 μm	R3	6	Kao, minor qtz	0.59	19.0
CS-2 vein	R3	6	Kao, qtz, uk	0.47	0.3
CS-7 WR	R3	4	Kao, qtz, uk	0.35	5.7
CS-9 <2 μm fault	R3	5	Kao, minor qtz, uk	0.52	5.7
CS-11 <2 μm	R3	7	Kao	0.55	15.7
CS-13 <2 μm	R3	7	Kao	0.65	6.7
CS-14 <2 μm	R3	4	Kao, minor qtz, uk	0.41	0.9
CS-15 <2 μm	R3	5	Kao, minor qtz	0.53	1.6
CS-15 vein	R3	10	Kao, uk	0.51	0.4
CS-18 <2 μm	R3	5	Kao, minor qtz	0.47	5.3
CC-21 <2 μm	R3	4	Kao, qtz	0.43	6.7
CS-23 <2 μm	R3	5	Kao, qtz	0.51	5.3
CS-25 <2 μm	R3	4	Kao	0.47	1.6
CS-28 <2 μm fault	R1	23	Kao, qtz		
CS-30 <2 μm fault	R3/R1	10	Kao, qtz	1.05	19.0
CS-33 <2 μm	R3	5	Kao, qtz	0.5	15.7
CS-34 <2 μm	R3	5	Kao, minor qtz, uk	0.46	4.9
BY-1 <2 μm	R3	5	Minor kao	0.51	49.0
BY-2 <2 μm	R3	4	Minor kao	0.40	32.0
BY-3 <2 μm	R3	5	Minor kao	0.47	32.0
Sacramento pit					
SAC-1 vein fault	R3	5	Kao, qtz, chl, uk		
SAC-5 vein fault	R3	4	Kao, qtz, uk		
SAC-1 vein	R3	4	Kao	0.43	0.3
SAC-HFZ-5 vein	R3	4	Kao	0.40	1.9
S-1 <2 μm	R1	23	Kao, minor qtz		
S-2 <2 μm	R1	23	Kao		
S-3 <2 μm	R0/R1	30	Kao, minor qtz		
S-4 <2 μm	R1	33	Kao		
S-6 <2 μm	R3	5	Kao		
S-8 <2 μm	R3	5	Kao, qtz		
Mercur pit Mercur beds					
MB-1 <2 μm	R3	5	Minor qtz, uk	0.49	
MB-2 <2 μm	R3	4		0.46	
MB-3 <2 μm	R3	5	Minor qtz	0.51	
MB-3 WR	R3	4	Qtz, minor kao	0.37	99.0
MB-5 <2 μm	R3	5	Minor qtz, uk	0.54	
MB-5 WR	R3	5	Minor kao, uk	0.48	99.0
MB-6 <2 μm	R3	6	Minor qtz, uk	0.55	
MB-6 WR	R3	5	Minor kao, qtz, uk	0.51	99.0
MB-7 <2 μm	R3	6	Minor kao, minor qtz	0.59	11.5
MB-7 WR	R3	5	Qtz, minor kao, uk	0.45	99.0
MB-9 <2 μm	R3	4	Minor qtz, uk	0.43	
MB-9 WR	R3	4	Qtz, minor kao, uk	0.41	99.0
Mercur pit Magazine sandstone					
MM-1 <2 μm	R3	4	Minor qtz, uk	0.38	
MM-11 <2 μm	R3	4	Minor qtz	0.40	
MM-12 <2 μm	R3	4	Minor kao	0.42	99.0
MM-13 <2 μm	R3	4	Minor kao	0.38	13.3
MM-14 <2 μm	R3	4	Minor kao	0.41	99.0
MM-15 <2 μm	R3	6	Minor kao	0.56	99.0
MM-16 <2 μm	R3	4	Minor kao	0.43	13.3

TABLE 1. (Cont.)

Sample	I-S ordering	Minimum % smectite	Other minerals	Kubler index (°2θ)	Illite/kaolinite ratio (wt %)
Veins from altered Long Trail Shale					
FM-2	R3	2	Kao, qtz, minor R1	0.28	99.0
FM-3	R3	4	Kao, minor R1, Fe ox	0.32	7.3
FM-6	R3	2	Minor kao & R1	0.28	99.0
FM-7	R3	2	Qtz, minor R1 & kao	0.30	99.0
FM-9	R3	5	Kao, qtz	0.52	99.0
O-2	R3	4	Kao, qtz	0.46	4.0
CC-2	R3	4	Qtz, Fe ox	0.44	15.7
LT-3	R3	5	Kao, qtz, chl	0.52	13.3
LT-7	R3	5	Kao, qtz, R1	0.55	9.0
MLT-11	R3	4	Kao, py, chl, gyp, uk	0.34	

chl = chlorite, gyp = gypsum, I = illite, kao = kaolinite, ox = oxide, py = pyrite, qtz = quartz, R1 = R1-type illite-smectite, uk = unknown mineral tentatively identified as an Fe arsenate, WR = whole rock

and (002) and between the (002) and (003) diffraction peaks. The positions of these peaks are dependent on the smectite content of the illite-smectite phase.

Geochemical analyses

Pulverized samples of whole rock were analyzed for major and trace elements by Nuclear Activation Services Incorporated (Ann Arbor, Michigan) using X-ray fluorescence and neutron activation.

K-Ar age determinations of clay-size, illite-rich concentrates of shales, veins, and argillically altered limestone were done by Krueger Enterprises, Inc. (Cambridge, Massachusetts). Separates of the <2-μm-size fractions of altered limestones were chosen for K-Ar analysis because this size fraction was the smallest in which sufficient material could be obtained from all samples, thereby allowing meaningful comparison of the resulting ages. This size fraction is fine enough to concentrate the illite and remove much of the quartz. Four samples of 0.03- to 0.3-μm- and on a sample of <0.03-μm-sized material were also dated to determine any variation in age between the size fractions.

Argillic Alteration of Great Blue Limestone within the Mercur Deposits

Much of the gold mineralization within the Mercur district occurs within argillically altered Great Blue Limestone. The degree of argillic alteration varies widely within the Mercur deposits from precipitation of clay minerals in voids visible only in thin section to complete replacement of limestone by clay minerals and quartz over areas covering hundreds of square meters. Highly argillized limestone is uncommon in outcrops outside of the mined pits (Jewell and Parry, 1987; this study).

Alteration mineralogy

Previous studies of the argillic alteration at Mercur indicate that the mineralogy consists of illite + kaolinite + quartz + pyrite or Fe oxides (Jewell, 1984; Jewell and Parry, 1987; Tafuri, 1987). The results of this study confirm this suite of hydrothermal minerals. Along a traverse that crosses the Carrie Steele fault, where the host rock is the upper bed of the

Great Blue Limestone (CS and BY series samples; Fig. 4), argillic alteration has removed all of the calcite and the rock is 95 to 100 percent clay minerals and quartz. X-ray diffraction data from both the whole rock and <2-μm-size fraction of the rocks indicate that the illite is an R3 interstratification with <10 percent smectite (Table 1). The typical mineralogy of the <2-μm-size fraction is R3 interstratified illite-smectite (<10% smectite) + kaolinite + quartz (Fig. 7D, Table 1). This same mineralogy was observed in the whole rock and <2-μm-size fractions of the altered limestones of the Mercur beds (MB series samples) and the altered Magazine sandstone (MM series samples) within the Mercur pit. An XRD peak at 2.80 Å is commonly present indicating that the illites are a 2M₁ polytype, consistent with a hydrothermal or metamorphic origin. Clay minerals from unaltered limestones in the vicinity of the Mercur deposits include R1 illite-smectite with approximately 30 percent smectite. From microprobe analyses of the illite-smectite in unaltered limestone, we calculate that it contains 0.49 K per formula unit compared to 0.70 to 0.78 K in illites from argillically altered limestone (Jewell and Parry, 1988), indicating a much higher smectite content in the illitic minerals of the unaltered rocks.

Smectite-rich, R1 illite-smectite (20–30% smectite) was also observed in two samples from the Marion Hill pit, and from several samples in a traverse near the contact of the Eagle Hill Rhyolite in the Sacramento pit (Table 1). In the Marion Hill pit, the R1-type illite-smectite was found on the south strand of the Carrie Steele fault. In the Sacramento pit, the illite-smectite becomes more illite rich with distance from the contact of the Eagle Hill Rhyolite (SS series samples) and changes from type R1 to R3. Where R1 illite-smectite occurs, the host-rock lithology appears to have originally been a shale and the host-rock mineralogy may be an important control on alteration mineralogy in addition to proximity to other geologic features.

Illite textures in argillized limestones from the Mercur mine indicate a hydrothermal origin. These textures include illite flakes that radiate from a common center (Fig. 8A), an illite matrix consisting of a felted mesh of microlites that are interwoven in unoriented fashion (Fig. 8A), crosscutting microveinlets of illite (Fig. 8B), replacement of fossils by
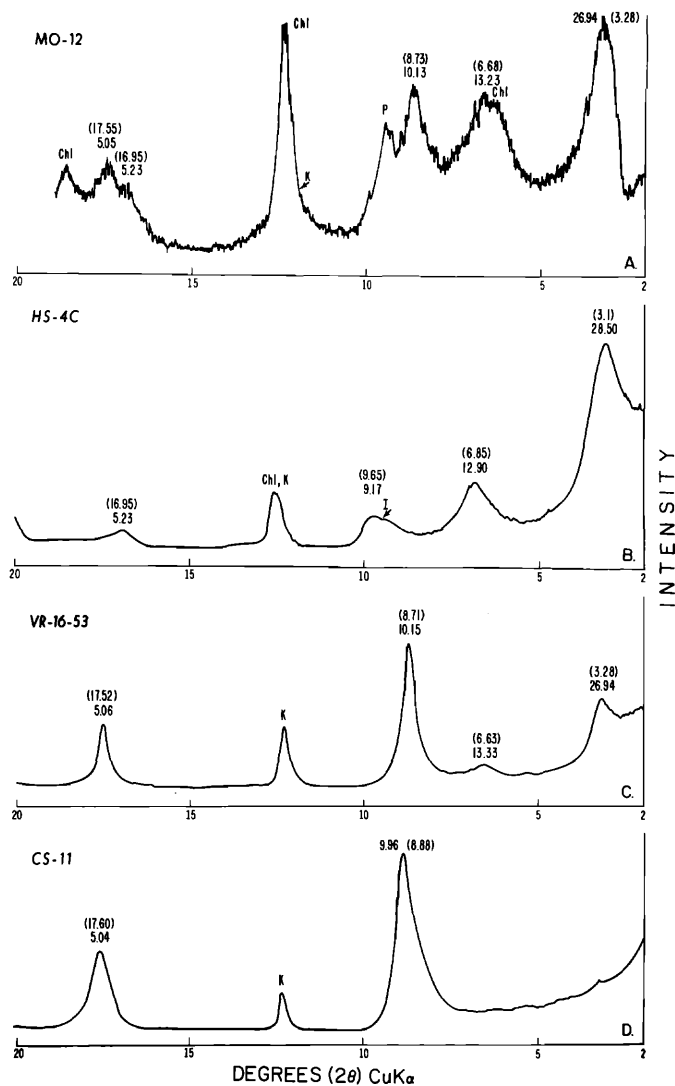
FIG. 7.   X-ray diffraction patterns from 2° to −20 ° 2θ showing low-angle peak positions of different types of illite-smectite. Patterns shown reflect decreasing amounts of smectite from top to bottom. A. Sample MO-12, <4 μm, from the Manning Canyon Shale, R1-type illite-smectite, 45 percent smectite + R3-type illite-smectite + pyrophyllite + chlorite + kaolinite. B. Sample HS-4C, <4 μm, from relatively unaltered Long Trail Shale, Mercur mine, R1-type illite-smectite, 33 percent smectite + R3-type illite-smectite (shown as I) + kaolinite + chlorite. C. Sample VR-16-53, <2 μm, from highly altered Long Trail Shale, Mercur mine, R3-type illite-smectite, 5 percent smectite + R1-type illite-smectite, 25 percent smectite + kaolinite. D. Sample CS-11, <2 μm, highly argillized limestone from Carrie Steele fault, R3-type illite-smectite, 7 percent smectite + kaolinite. The 2.80 Å peaks do not appear in this 2θ range.

kaolinite and/or illite (Fig. 8C), and irregular, fractured, and corroded quartz grains with intergrown illite. Crosscutting irregular zones also contain kaolinite and illite in a felted texture. Some larger illite grains contain interlamellar kaolinite. Pods up to 1 cm in diameter containing coarse blocky illite, quartz, and kaolinite are common (Fig. 8D). Thin section analysis indicates that multiple stages of argillic alteration occurred. Early kaolinite + quartz is accompanied by organic material and veins of pyrite + kaolinite + quartz in unoxidized rock. A second and pervasive stage is composed of illite

+ kaolinite + quartz ± rutile (?). A third stage, which also consists of illite + kaolinite + quartz, generally has a higher illite/kaolinite ratio than stage 2 and occurs as either replacement of the stage 2 or as crosscutting veins (Fig. 8B).

Argillic alteration of limestone also has resulted in phyllosilicate vein formation and fossil replacement very similar to that seen in altered Long Trail Shale throughout the southern Oquirrh Mountains (Wilson and Parry, 1990a; Wilson et al., 1992). This type of vein formation differs from microveinlet formation in that it is obvious in outcrop. In the Carrie Steele fault samples, the veins are generally a few millimeters wide and extend only a few centimeters vertically or along strike. Fossil replacement is complete, but the original fossil is often identifiable. Most clay veins consist of illite + kaolinite + quartz ± chlorite, pyrite or Fe oxides, and other unidentified phases (Table 1). Illitic material in the veins is also an R3 illite-smectite (<10% smectite). Veins from the Herschel fault zone (Sacramento pit, samples SAC-HFZ-5 and SAC-1) are more extensive, on the order of meters long and up to 0.5 cm wide, but have a mineralogy similar to that of the Carrie Steele veins (CS-2, CS-15). Vein orientation was difficult to measure, but veins were subparallel to faults. Illite XRD spacings of (001) planes greater than 10.05 Å suggest that some of the vein illite from both areas is ammonium bearing.

Illite/kaolinite ratios: Estimates of relative abundance of illite and kaolinite of the clay-size fraction were made based on the XRD method described by Moore and Reynolds (1989, p. 297). The illite/kaolinite ratio is variable throughout the two deposits and between the veins and the rock hosting them (Table 1).

The illite/kaolinite ratio of the <2-μm-size fraction of samples along the Carrie Steele fault varies from 49 to 0.89 (Table 1). Within about 50 m of the two strands of the Carrie Steele fault (Fig. 4), the <2-μm clay mineralogy averages 90 percent illite and 10 percent kaolinite; beyond about 50 m, the illite/kaolinite ratio is approximately one. In sample CS-15, the one sample in which uncontaminated vein material could be separated from the host rock, the illite/kaolinite ratio was much greater in the vein than in the <2-μm-size fraction of the rock matrix. The highest illite/kaolinite ratios from the Marion Hill pit were obtained from samples collected from a northwest-trending high-angle fault west of the Carrie Steele fault (Fig. 4). The <2-μm separates of these samples are almost pure illite. Illite/kaolinite ratios from the altered Mercur beds and Magazine sandstone from the Mercur pit (MB and MM series samples) are higher and more consistent than those from the Marion Hill pit (CS series samples). Within the Mercur pit, the illite/kaolinite ratios from the <2-μm fractions of both units are 32 or greater, and many samples do not contain any kaolinite (Table 1). There is no discernible zoning of the illite/kaolinite ratio on the Lulu Graben fault. A comparison of the illite/kaolinite data with Au concentrations within all the samples suggests that higher gold values are associated with higher illite/kaolinite ratios, but this trend is not consistent.

The illite/kaolinite ratios of whole-rock samples were determined from modal analyses calculations using the program MODECALC, a calculation of mineral abundance from a least squares fit of mineral chemical composition and rock
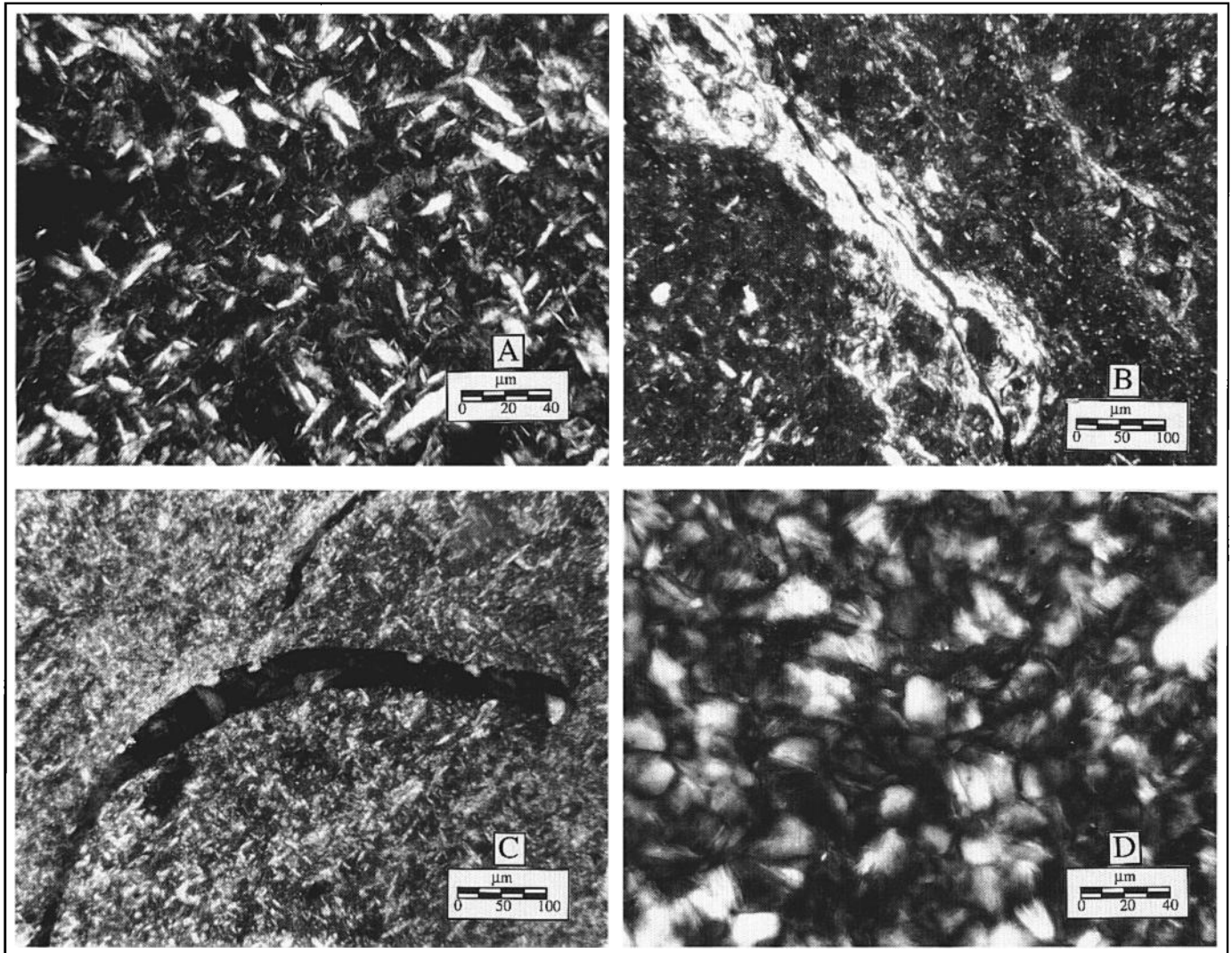
FIG. 8. Photomicrographs of hydrothermal textures in argillically altered limestone in the Mercur deposits. A. Felted texture of intergrown illite, sample CS-9. B. Veinlet of R3-type illite-smectite, sample CS-7. C. Brachiopod (?) fossil replaced by kaolinite and surrounded by illite with a felted texture, sample CS-9. D. Intergrown kaolinite crystals, sample CS-5.

chemical composition (Parry et al., 1980). These illite/kaolinite ratios are also variable, but are consistently lower than in the <2-μ- size fractions (Tables 1 and 2) and show that illite is more abundant in the finer size fractions of the rock. This is consistent with illite/kaolinite ratios observed in thin section.

Kubler index: The Kubler illite crystallinity index of <2-μm-size separates of Mercur mine samples and the crystallinity index of illitic veins from throughout the region are listed in Table 1. Kubler indices of the <2-μm-size separates range from 0.35 to 0.59 with a single sample (CS-30) at 1.09. The Kubler index of vein illites is 0.28 to 0.52. These ranges are consistent with illite of hydrothermal origin, low-smectite content, and low variation in particle size. The single measurement above 0.6 corresponds to the highest grade of diagenesis.

Summary of illite data: Analysis of the type of illite-smectite mineral present in the argillic alteration of the limestones at

Mercur, the percent smectite interstratified with illite in the minerals, and the Kubler index indicates that the mineralogy of the alteration within the deposits is very consistent. The argillic alteration is dominated by an R3 mineral that is <10 percent smectite. This illite occurs with kaolinite, quartz, and pyrite or Fe oxides. The amount of smectite in the minerals was constant irrespective of the size fraction of the sample analyzed (0.03 μm to whole rock). Kubler index values are consistent with a hydrothermal origin. There was no discernible relationship between the Kubler index and Au values, nor was zoning of the Kubler index apparent within the immediate vicinity of the Carrie Steele or Lulu Graben faults.

Comparison with other deposits: Comparison of the argillic alteration at Mercur with that at other sediment-hosted disseminated gold deposits is difficult because the clay mineralogy has not been similarly characterized elsewhere. In particular, the mineral referred to as "illite" or "sericite" in these

TABLE 2. Modal Mineralogy of Whole-Rock Samples

Sample no.	Quartz	Hematite	Calcite	Pyrite	Kaolinite	Dolomite	Illite	Barite	Illite-kaolinite
CS-1	45.5	3.6		0.2	16.5		33.3		2.03
CS-5B	25.9			9.8	50.1		9.5		0.19
CS-9	45.0	6.7		0.1	30.3		16.7		0.56
CS-11	53.5	4.7		0.1	23.1		17.7		0.81
CS-13	47.4	6.4		0.1	25.5		20.4		0.81
CS-14	72.3	4.3		0.1	19.4		3.0		0.15
CS-15	50.4	13.0		0.4	23.9		10.3		0.43
CS-18	66.4	5.0		0.1	17.0		9.6		0.56
CS-21	76.0	2.9		0.4	11.1		8.3		0.75
CS-24	72.1	2.2		0.2	16.3		8.1		0.49
CS-27	47.5	4.5			17.6		29.8		1.70
CS-28	39.4			0.4	18.5		38.6		2.13
CS-29	38.2	2.6		6.2	23.6		26.0		1.08
BY-1	58.9			0.4	11.7		28.3		2.45
MM-1	56.8	1.9		4.3			14.7	21.0	
MM-12	59.8	1.7		7.4	2.8		27.9		10.1
MM-15	57.8	1.3		0.1	3.6		36.3		10.1
MM-16	56.9		25.5		5.0		11.5		2.33
MB-1	40.7		41.6	0.2	2.4		12.9		5.25
MB-2	59.2		3.1	0.1	1.6		34.1		24.0
MB-3	71.2		1.9	4.2	4.3		16.2		7.18
MB-5	44.4		31.7	4.7	4.6	1.8	10.6		2.33
MB-6	31.4		41.6	1.8	2.4	3.5	18.7		6.69
MB-7	37.2		8.1	7.0	16.2		26.5		1.63
MB-9	36.7		23.2	3.9	6.9	2.0	24.4		3.55

Determined using computer program MODECALC (Parry et al., 1980)

studies is not characterized in terms of smectite content. In general, "illite" + kaolinite + quartz is a common alteration assemblage in sediment-hosted disseminated gold deposits, but there is a great variation in the abundance of illite and kaolinite and in the distribution of these minerals in relationship to features thought to have controlled migration of mineralizing fluids. The predominant clay minerals in the Carlin deposit are 1M and 2M illite and variable amounts of kaolinite (Bakken et al., 1989). The alteration is zoned with jasperoid and kaolinite (dickite) abundant near fluid conduits surrounded by an envelope of illitic alteration (Kuehn and Rose, 1992). In the nearby Post-Betze deposit, mineralization is also controlled by faults and a kaolinite (dickite)-rich core is surrounded by kaolinite and sericite. Only a few samples have abundant hydrothermal illite, but the <2-μm fraction of these samples is interpreted as mostly hydrothermal illite that probably formed as a result of gold-related alteration (Arehart et al., 1993). Kaolinite is the principal clay introduced at Alligator Ridge where the unaltered host Pilot shale contains 30 to 40 percent illite (Ilchik, 1990). At the Barney's Canyon deposits, Utah, the alteration assemblage is R3-type illite-smectite + kaolinite + quartz (Presnell and Parry, 1992). There is a zoning of the clay mineralogy within the orebody, which consists of an illite-rich core surrounded by a kaolinite-rich zone. As at Mercur, the illitic minerals have a low smectite content.

Chemical composition of altered rock

Major element analyses of altered rock (Table 3) were used to estimate the extent of calcite removal and to estimate modal mineralogy. Comparison of the major element chemistry of samples from this study with unaltered massive limestone and silty limestone compositions of Jewell and Parry (1988) shows considerable chemical changes within the limestone Upper beds unit in the Marion Hill pit sample series which transects the Carrie Steele fault (Table 3). Comparison of the Carrie Steele suite (CS samples) with the chemical composition of either type of unaltered rock shows highly enriched Al_2O_3 and SiO_2 values and extreme depletion of CaO, indicating extensive loss of the original calcite and at least partial replacement by illite, kaolinite, and quartz. This is reflected in the whole-rock modal analyses presented in Table 2. The amount of illite present is indicated by the K_2O and Na_2O concentrations, but because of the probable presence of NH_4 in the illite, estimates of illite content of the rock are minimum values (Table 2).

Limestone hand specimen samples from the Lulu Graben do not appear as extensively altered as those of the Marion Hill pit. Altered Mercur beds samples (MB series, Figs. 5 and 6) were probably originally silty limestone and the sample suite shows variable CaO, SiO_2, and Al_2O_3 values with distance from the north strand of the Lulu Graben. CaO values range from 0.73 to 24.60 wt percent. Several of the Mercur beds (MB) samples have low totals in major element chemistry. This may be due in part to the presence of an Fe arsenate mineral which was tentatively identified in the XRD patterns and the As content for these samples (Table 3).

Altered Magazine sandstone samples (MM series, Fig. 5) are from a sample suite which extends across the Lulu fault zone. In hand specimen these samples are extremely argillized. Modal and XRD analyses indicate a low kaolinite content for the MM series samples (Tables 1 and 2).

Altered rocks in the Mercur mine contain anomalous concentrations of As, Au, Ba, Hg, S, Sb, and Tl (Table 3). The

TABLE 3. Major, Minor, and Trace Element Data for Argillically Altered Rocks from Ore Zones

Sample no.	SiO$_2$	Al$_2$O$_3$	CaO	MgO	Na$_2$O	K$_2$O	Fe$_2$O$_3$	As	Au	Ba	Hg	S	Sb	Tl
CS-9	67.10	16.20	0.19	0.42	0.15	1.49	7.21	1,800	<1	310	2	700	200	16
CS-11	72.90	13.80	0.07	0.58	0.02	1.70	5.20	680	3	240	1	300	120	8
CS-13	68.00	15.20	0.08	0.63	0.04	1.93	6.87	360	1	230	<1	400	19	2
CS-14	82.90	8.00	0.02	0.18	<0.01	0.27	4.45	510	5	140	<1	300	34	2
CS-15	66.70	11.20	0.02	0.32	0.12	1.06	13.60	660	2	200	3	2,000	46	<2
BY-1	77.90	12.60	0.11	0.86	0.06	2.44	1.41	360	6	390	7	1,400	56	36
CS-5B	53.80	20.90	0.34	0.33	0.93	0.87	6.68	210	8	210	2	54,000	12	12
CS-1	69.10	15.80	0.16	0.88	0.10	3.13	4.64	1,700	42	540	10	1,200	12	320
CS-18	78.80	8.85	0.82	0.44	0.05	0.89	5.29	7,800	640	230	1	200	22	66
CS-21	85.40	6.26	0.11	0.33	0.11	0.81	3.42	1,800	130	210	<1	2,000	10	110
CS-24	83.50	8.29	0.05	0.27	0.07	0.74	2.60	840	4,900	200	4	1,100	22	220
CS-27	70.00	15.40	0.06	0.73	0.11	2.69	5.37	410	45	370	2	200	44	120
CS-28	69.60	19.00	0.28	0.47	1.09	1.74	0.97	200	5	230	1	1,100	61	12
CS-29B	63.50	16.70	0.15	0.42	0.93	1.10	6.70	1,000	5	160	<1	33,000	85	12
MB-1	47.40	4.36	24.60	0.72	<0.01	1.13	1.99	7,400	770	100	8	500	INT[2]	26
MB-2	75.70	10.60	2.14	0.84	0.03	2.78	2.88	900	570	400	4	300	51	50
MB-3	80.90	6.26	0.73	0.42	0.03	1.59	3.45	370	740	200	<1	21,000	16	76
MB-5	51.50	4.95	19.30	0.57	<0.01	1.19	2.63	460	540	120	1	40,000	5.7	46
MB-6	40.30	6.61	25.40	1.09	0.05	1.58	1.69	11,000	47	80	3	9,900	INT[2]	18
MB-7	55.10	12.00	3.95	1.14	0.14	2.91	5.19	24,000	1,900	1,300	19	36,000	INT[2]	160
MB-9	50.80	10.10	17.60	1.16	0.06	2.06	3.24	290	2	150	4	20,000	0.8	22
MM-1	61.90	3.87	0.72	0.16	0.17	1.73	5.00	920	810	120,000	5	39,000	520	120
MM-12	73.70	9.57	4.39	0.83	0.06	2.35	2.47	740	86	550	1	800	33	46
MM-15	75.40	11.60	1.34	1.06	0.08	3.16	1.43	120	180	650	<1	200	56	82
MM-16	64.90	5.41	15.90	0.56	<0.01	1.17	0.26	37	5,000	160	<1	200	8.4	50
Massive limestone[1]	6.42	1.01	50.65	0.39	0.00	0.11	0.89							
Silty limestone[1]	34.55	5.99	29.37	0.72	0.05	1.01	2.12							

[1] Unaltered rock analyses from (Jewell and Parry, 1988)
[2] No analysis because of interference

concentration of these elements vary erratically. Au varies from <1 ppb to 5 ppm, As varies from 37 to 24,000 ppm, Hg varies from 1 to 47 ppm, and Tl varies from 2 to 320 ppm. All the data from the Mercur deposits are from mineralized rock, and the considerable variation in the heavy metal content, particularly Au, is typical for sediment-hosted disseminated gold deposits (Ashton, 1989).

Alteration Mineralogy of the Long Trail Shale

Regional-scale hydrothermal alteration of the Long Trail Shale occurs throughout the southern Oquirrh Mountains. Alteration in the shale is recognizable by the phyllosilicate mineralogy, mineral textures, the presence of illite-rich veins, and the chemical composition of the rocks.

The alteration mineralogy of the Long Trail Shale varies from a relatively diverse assemblage accompanying R1 illite-smectite to a more limited assemblage that accompanies R3 illite-smectite (Wilson, 1992). Long Trail Shale containing R1 illite-smectite (20–35% S; Fig. 7A) is usually black and contains kaolinite + chlorite + quartz + up to 3.4 percent organic carbon ± calcite, pyrite, dolomite, or halloysite. Some Long Trail Shale samples contain both illite types. The R1 illite-smectite assemblage commonly occurs in the Long Trail Shale within the vicinity of the Mercur and Sacramento pits. The R1 illite in the Long Trail shale is similar to R1 illites in shale horizons within the limestones of the gold deposits.

The R3 illite-smectite assemblage is the most common in the Long Trail Shale and consists of R3 illite-smectite (5–10% smectite; Fig. 7D) + kaolinite + quartz ± Fe oxides. It is found near and stratigraphically above gold mineraliza-

tion on the south side of Ophir Canyon, between Ophir Canyon and Mercur, at West Dip, and at Sunshine Canyon (Fig. 1). The R3 assemblage is also found in the region of Clay Canyon south to Five Mile Pass where high gold values are known (Bill Tafuri, unpub. data). This assemblage is commonly accompanied by heavy metal-rich veins consisting of NH$_4$-rich R3 illite-smectite + kaolinite + quartz ± Fe oxides and chlorite. Podlike replacements of fossils containing the same mineralogy are also common (Wilson and Parry, 1990a; Wilson et al., 1992). The heavy metals associated with these veins are Au, As, Hg, Tl, Mo, Sc, Se, and Cu (Wilson and Parry, 1990b). Long Trail Shale that consists of this R3 illite-smectite + kaolinite + quartz assemblage also is usually enriched in these same heavy metals compared to shale containing R1 illite-smectite (Table 3).

The XRD traces shown in Figure 7 demonstrate the progressive change in the illite-smectite mineralogy with increasing degree of hydrothermal alteration. Figure 7B is representative of relatively unaltered Long Trail Shale and shale horizons from within the altered limestones in the deposits which contain R1 illite-smectite . Figure 7C is representative of a high degree of shale alteration characterized by R3 illite-smectite. Figure 7D is an XRD trace of argillically altered limestone that is also representative of the most highly altered Long Trail Shale where the clay mineralogy is limited to R3 illite-smectite in association with kaolinite. Within the Long Trail Shale, this assemblage is found in association with NH$_4$-rich illite veins.

Figure 9A is a Watanabe plot of diffraction data of illitic material from the Long Trail Shale. Unmineralized, heavy
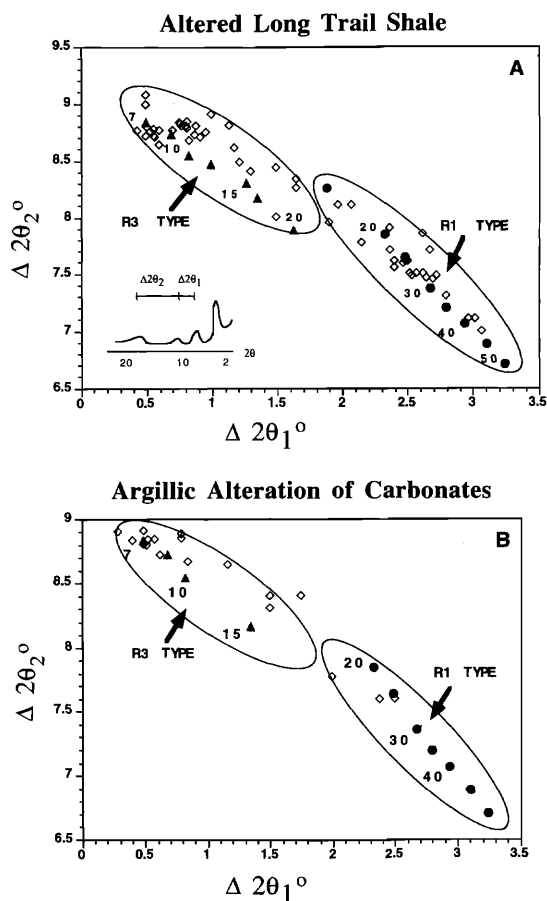
FIG. 9. Watanabe diagrams showing smectite content of R1-and R3-type illite-smectite for (A) Long Trail Shale and (B) argillically altered limestones from the orebodies. The filled circles and triangles show where illite-smectite phases of different smectite content plot as determined from NEWMOD simulations (Reynolds, 1985). The numbered labels indicate percent smectite in the illite-smectite. Open diamonds are data from this study. The ellipses indicate the fields of R1- and R3-type illite-smectite.

metal-poor Long Trail Shale plots on the R1 ordering trend with relatively high amounts of smectite. In comparison, heavy metal-rich Long Trail Shale plots on the R3 trend with low amounts of smectite in the illite-smectite minerals. The minor variation in the smectite content of the R3-ordered illite-smectite is also shown.

Comparison of argillic alteration in the Mercur deposits and in the Long Trail Shale

Hydrothermally altered Long Trail Shale from throughout the southern Oquirrh Mountains has a more diverse alteration mineralogy than the argillically altered limestones within the gold deposits. However, Long Trail Shale from areas enriched in heavy metals and/or near gold mineralization consists of the same mineralogy as the argillically altered limestones in the gold deposits. The whole-rock and minor element chemistries of the two altered rock types are notably similar (Table 3). Hydrothermal features such as heavy metal-rich veins, fossil replacement by the same minerals which occupy veins, felted textures of clay minerals, and other textures previously

discussed are common to both Long Trail Shale and the argillized limestone of the deposits.

We have interpreted the mineralogical, textural, and chemical similarities between the argillic alteration of limestones in the Mercur deposits and the Long Trail Shale with the R3 illite mineral assemblage as indicating that shale with the R3 assemblage has undergone the most intense hydrothermal alteration. Thus the variation in alteration intensity within the Long Trail Shale is best defined by the illite-smectite mineralogy and by the increase in illite content of the illite-smectite minerals with increase in alteration intensity as shown on the Watanabe diagram for the Long Trail Shale (Fig. 9A).

Argillically altered limestones of the gold deposits plot at the upper left end of this trend (Fig. 9B), with most samples containing an R3 illite-smectite (3–10% smectite). These highly altered limestones also contain veins of R3 illite-smectite (2–7% smectite) + kaolinite + quartz that are similar to veins found in the most intensely altered Long Trail Shale. Argillic alteration from within the gold deposits only rarely includes the high smectite illite-smectite (25–33% smectite) similar to that observed in less altered Long Trail Shale. This high smectite illite-smectite was observed only in altered shale horizons within the limestone.

The mineralogical, textural, and chemical similarities between the highly altered Long Trail Shale and argillic alteration of limestone within the Mercur deposits are considerable, particularly in view of the differences in the original rock type. This evidence suggests that the same alteration event was responsible for both the R3-type argillic alteration in the Mercur deposits and in the Long Trail Shale.

K-Ar Data

Chronological information is essential to construction of a genetic model for the formation of the Mercur gold deposits. To obtain this information, K-Ar ages of illite from highly argillically altered and mineralized limestones from within the Mercur deposit were determined. The age data are integrated with mineralogical, petrographic, thermal, and geologic information in order to estimate the age of the gold mineralization and to test the proposed relationship between the regional hydrothermal alteration of shales and the argillic alteration of limestones within the Mercur deposits.

As previously discussed, several characteristics of sediment-hosted disseminated gold deposits have made their ages extremely difficult to determine. Although these same problems exist at Mercur, K-Ar ages of illite-rich clay-size separates from argillic alteration within the deposits and K-Ar ages of clay separates and veins in nearby Long Trail Shale provide good evidence for the general age of gold mineralization for the following reasons: (1) textural evidence and the occurrence of illite in veins indicates a hydrothermal origin for illite; (2) illite-rich argillic alteration was observed within strongly mineralized areas of the ore bodies; (3) illite clay is capable of recording the chemical, tectono-thermal event related to ore formation; (4) no petrographic or XRD evidence indicates the presence of feldspars or other K-bearing minerals in dated material; and (5) the similar alteration characteristics between mineralized limestone in the deposits and altered Long Trail Shale in the district allow comparison of

TABLE 4. K-Ar Ages of Mercur Argillic Alteration

Sample	Average $^{40}Ar^*/^{40}Ar$ total	Average % K	$^{40}Ar^*$ (ppm)	^{40}K (ppm)	Age (Ma)	Modeled clay mineralogy
Carrie Steele fault suite						
Upper bed series						
CS-9 <2 μm	0.787	2.553	0.03105	3.046	167 ± 4	85% R3 I-S, 15% kao
CS-11 <2 μm	0.904	4.894	0.06450	5.839	181 ± 4	93% R3 I-S, 7% kao
CS-13 <2 μm	0.896	4.441	0.05757	5.298	178 ± 4	87% R3 I-S, 13% kao
CS-14 <2 μm	0.708	1.375	0.02194	1.640	217 ± 5	47% R3 I-S, 53% kao
BY-1 <2 μm	0.908	6.154	0.09220	7.342	204 ± 4	98% R3 I-S, 2% kao
CS-9 0.03–0.3 μm	0.850	3.569	0.03910	4.258	152 ± 4	
CS-14 0.03–0.3 μm	0.655	2.155	0.02837	2.570	181 ± 5	
Lulu Graben suite, Mercur pit						
Mercur beds series						
MB-1 <2 μm	0.858	5.796	0.04861	6.914	117 ± 3	100% R3 I-S
MB-2 <2 μm	0.917	6.859	0.07404	8.183	149 ± 3	100% R3 I-S
MB-6 <2 μm	0.819	5.431	0.05394	6.479	138 ± 3	100% R3 I-S
MB-1 0.03–0.3 μm	0.856	6.209	0.04354	7.407	98.4 ± 3	
Magazine Sandstone Series						
MM-1 <2 μm	0.930	5.772	0.09439	6.886	222 ± 5	100% R3 I-S
MM-15 <2 μm	0.945	7.093	0.11860	8.461	226 ± 5	99% R3 I-S, 1% kao
MM-15 0.03–0.3 μm	0.952	7.076	0.10920	8.441	210 ± 5	
Vein illite in Long Trail Shale						
LT-3	0.676	2.352	0.02053	2.806	122 ± 5	93% R3 I-S, 7% kao
FM-3	0.879	2.721	0.03766	3.246	189 ± 7	88% R3 I-S, 12% kao
FM-9	0.795	3.068	0.03786	3.660	170 ± 6	99% R3 I-S, 1% kao
O-2 and O-3	0.797	2.726	0.03088	3.252	156 ± 6	80% R3 I-S, 20% kao
CC-2	0.497	1.333	0.01715	1.590	177 ± 7	94% R3 I-S, 6% kao
MLT-11	0.762	2.164	0.02291	2.582	147 ± 6	
Clay-size separates from Long-Trail Shale						
MS-8 <2 μm	0.624	4.169	0.05050	4.974	167 ± 6	93% R3 I-S, 7% chl
LT-9 <2 μm	0.5105	2.826	0.03363	3.371	164 ± 6	87% R3 I-S, 13% R1 I-S
MC-7-19 <10 μm	0.2205	1.099	0.01264	1.311	159 ± 7	38% R3 I-S, 32% R1 I-S, 30% kao
VR-16-53 <2 μm	0.629	3.217	0.03765	3.837	161 ± 6	78% R3 I-S, 15% kao, 7% R1 I-S
O-5 <2 μm	0.475	1.258	0.01118	1.500	124 ± 5	40% R3 I-S, 32% kao, 28% R1 I-S
CC-2 <4 μm	0.719	2.801	0.03950	3.342	193 ± 7	100% R3 I-S
West dip samples						
WD-59 0.03–0.3 μm	0.718	2.509	0.02495	2.993	138 ± 4	
WD-59 <0.03 μm	0.380	1.939	0.01684	2.313	121 ± 3	

Analyses by Geochron Laboratories, Inc.; λ = 0.581 × $10^{-10/yr}$, β = 4.962 × $10^{-10/yr}$, $^{40}K/K$ = 1.193 × $10^{-4 g/g}$
Abbreviations: chl = chorite, I-S = illite-smectite, kas = kaolinite

K-Ar dates, particularly with the dated illite veins from the shale.

K-Ar ages from the Mercur deposits

The K-Ar dates and related chemical data for samples of argillically altered limestone from within the gold deposits and from Long Trail Shale are shown in Table 4 and Figure 10. Dates from the Mercur deposits were obtained from both the Carrie Steele and the Lulu fault zones and range in age from 98.4 to 226 Ma. Two size fractions of the rock were dated. Most samples were the <2-μm-size fraction, which was the finest size fraction that could be extracted from all samples and which allowed for meaningful comparison of similar material between samples. The 0.03- to 0.3-μm-size

fraction of four samples was dated in order to test for age variation within individual samples. The histogram in Figure 10 shows the bimodal distribution of the data, with modes near 160 and 220 Ma.

The apparent ages from the Carrie Steele sample suite range from 217 to 152 Ma and become progressively younger as the fault is approached (Fig. 4, Table 4). Illite ages from the <2-μm-size fraction decrease from 217 Ma farthest from the fault (CS-14) to 167 Ma on the north strand itself (CS-9). The date from the northwest-trending cross fault is also relatively old at 204 Ma (BY-1). Ages of the 0.03- to 0.3-μm-size fraction from CS-9 and CS-14 are younger than the <2-μm-size fraction ages. The age of the 0.03- to 0.3-μm fraction from the Carrie Steele fault (CS-9) is 152 Ma. The difference

between the age of the 0.03- to 0.3-μm and <2-μm-size fractions in CS-9 is small and is almost within the analytical uncertainty. The age of the 0.03- to 0.3-μm-size fraction of CS-14 is 181 Ma which is considerably younger than the 217 Ma of the <2-μm-size fraction.

Dated samples from the Lulu Graben of the Mercur pit are from the Mercur beds, extending north from the north strand of the Lulu fault zone into relatively unaltered rock, and from the Magazine sandstone extending across the Lulu fault zone (Figs. 5 and 6). The Mercur beds samples have ages ranging from 98.4 to 149 Ma.; and the Magazine sandstone samples range from 210 to 226 Ma (Table 4). As in the case of the Carrie Steele fault, the 0.03- to 0.3-μm-size fractions dated from the Lulu Graben faults are also younger than the <2-μm-size fractions. In sample MB-1, the 0.03- to 0.3-μm-size fraction age is 98.4 Ma in comparison to the 117 Ma age of the <2-μm-size fraction. In sample MM-15, the 0.03- to 0.3-μm-size fraction age is 210 Ma, in comparison to 226 Ma for the <2-μm-size fraction.

K-Ar ages of the shales

K-Ar ages of vein illites and clay-sized, illite-rich separates of shales are also shown in Table 4 and Figure 10. Dates from the Long Trail Shale range from 121 to 193 Ma. Both the ages from the illite veins and from the clay-sized separates of the whole rock obtained from this unit averaged 160 Ma. Three dates from the Long Trail Shale were obtained from the Mercur mine: sample MLT-11, an illite-rich vein located 30 m from the Eagle Hill Rhyolite from within the Sacramento pit, dated at 147 ± 6 Ma; sample MC-7-19, a <10-μm-size separate of weakly mineralized, R1-type illite-smectite-rich, Long Trail Shale obtained from the bottom of the unit, dated at 159 ± 7 Ma; and sample VR-16-53, a highly altered, R3-type illite-smectite-rich, and weakly mineralized sample from the Violet Ray area to the south of the Sacramento pit (currently unmined), dated at 161 ± 6 Ma (Wilson and Parry, 1990a).

Interpretation of the Age Data

The range in ages, the difference in age between coarse and fine fractions of the same sample, and the variation in age with distance from the faults indicates that most of the dates are mixed ages that have resulted from superimposed geologic events. However, although many of the K-Ar ages are mixed, they are also fundamentally related to the thermal history of the host rocks which can be used to interpret the age data meaningfully. Mixed ages can result from three different processes: (1) a mixture of illites formed at different times, (2) incomplete Ar loss caused by reheating of an earlier formed illite resulting in partial resetting of the K-Ar age, and (3) cooling during uplift and exhumation of a sedimentary section. The apparent K-Ar ages may represent any combination of these processes. Observed geologic relationships in the region and modeling of Ar diffusion in illite have guided our interpretation of the age data.

Thermal history of the Mercur district

In addition to the hydrothermal activity responsible for gold mineralization at Mercur, other thermal events likely to have affected rocks of the Mercur district are (1) burial

metamorphism and other possible basin-related water/rock interactions during development of the Oquirrh basin, (2) tectonic thickening during orogenic events, and (3) Tertiary igneous activity.

Burial metamorphism: Prior to exhumation, the ore-bearing horizons in the Great Blue Limestone were overlain by 7.5 km of Pennsylvanian and Permian strata (Jordan and Douglass, 1980). Stratigraphic burial was at a maximum at about 260 Ma. The most notable mineralogical and chemical changes that accompany burial metamorphism are conversion of smectite to illite and a decrease in illite K-Ar ages with depth as clay minerals are recrystallized (i.e., Aronson and Hower, 1976; Boles and Franks, 1979; Pollastro, 1990). All of these studies indicate that the burial of sediments of the Mercur district to 7 km should have destroyed any detrital component in the <2-μm (and probably coarser) size fraction and converted all illitic minerals to R3 illite-smectite.

Tectonic thickening: Additional tectonic thickening of the stratigraphic section at Mercur occurred in Mesozoic time with the Cretaceous Sevier orogeny and an unnamed Jurassic tectonic event (Presnell et al., 1993; Presnell and Parry, in press). Paleozoic thermal gradients are unknown, but using a gradient of 33°C/km which is reasonable for similar modern environments, a temperature of 250°C is a minimum value for 7.5 km of burial. The temperature increase resulting from tectonic thickening of the sedimentary cover in Mesozoic time could have been as much as 75°C yielding a final temperature of approximately 325°C estimated from the numerical modeling and constrained by fluid inclusion observations of Yonkee et al. (1989). The Manning Canyon Shale, immediately above the upper member of the Great Blue, contains abundant pyrophyllite + kaolinite + quartz as vein fillings and in the shale matrix (Wilson and Parry, 1989). Calculation of pressure and temperature for the univariant reaction: kaolinite + 2 quartz = pyrophyllite + water from the thermodynamic parameters of Hemley et al. (1980) indicates a minimum temperature of 260°C. Hunziker et al. (1986) and Hunziker (1987) have shown that <2-μm illite ages are completely reset at 260° ± 30°C. As with stratigraphic burial, tectonic thickening should have reset K-Ar systematics of any detrital <2-μm component in the material dated in this study, and at these temperatures and depths, the illite-smectite mineral present should be a R3 with low smectite content. In addition, tectonic thickening would most likely have partially or wholly reset any ages which resulted from burial metamorphism.

Tertiary igneous activity: Intrusion of the Eagle Hill Rhyolite and the Porphyry Knob quartz monzonite are the youngest thermal events recognized in the Mercur district. The Eagle Hill rhyolite dike is 266 m thick and the thickest sill at Porphyry Knob is 122 m thick. For water-saturated rocks, the peak temperatures in surrounding country rock would have fallen to near ambient temperature within about 1.5 pluton diameters (Jaeger, 1959; Cathles, 1977) corresponding to a distance of about 400 m for the Eagle Hill rhyolite. The total rock cover in Tertiary time is unknown, but geologic reconstruction at Bingham, 25 km northeast of Mercur (Fig. 1), suggests that post-Tertiary erosion has removed about 800 m of sediment there and that ambient temperature at the time of rhyolite emplacement at Mercur was no higher than 50°C. This indicates that temperatures sufficiently high to
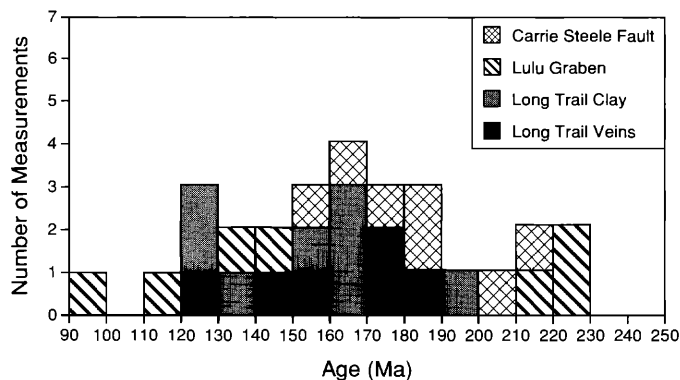
FIG. 10.   Histogram of age data.

reset <2-μm-sized illite would exist only within a few meters of the rhyolite contact. Fluid flow focused in faults or in exceptionally permeable horizons could have produced local variations. One illite vein within 30 m of the Eagle Hill contact has a K-Ar age of 147 ± 7 Ma. The mean age of illite veins in the southern Oquirrh mountains is 160 Ma (Wilson and Parry, 1990a) indicating minimal argon loss from sample MLT-11 due to any thermal effects of the intrusion. In addition, if the mixed ages were the result of precipitation of new illite or thermal resetting of previously existing illite as a result of the igneous intrusion, then the ages should vary systematically with respect to proximity to the igneous rocks. This relationship is not observed in either the limestone or shale.

Evaluation of mixed ages resulting from mixing of different age illites

K-Ar ages of finer size fractions of sedimentary clay are almost always younger than the coarser fractions which has led to the assumption that shale is a mixture of coarser detrital and finer diagenetic phases. Investigations by Pevear (1992), Mossman et al. (1992), and Mossman (1991) have shown that the different aged components can be mineralogically different and where this occurs, the relative proportions of each in a dated sample can be determined by x-ray diffraction techniques. For example, Pevear (1992) found shale samples from a 13,000-ft well near Pt. Thomson, Alaska, contained two components: a diagenetic young illite-smectite and older detrital illite. Plotting the proportions of each end member versus apparent K-Ar age yielded a mixing line and the age of each end member. In a similar series of studies by Moss-mann et al. (1992) and Mossmann (1991), sediments contained up to three distinct illite-smectite phases which could be resolved by X-ray diffraction measurements.

We tested the role of simple mixing of illite-smectite of two different ages as a cause for mixed ages in the Long Trail Shale samples. Samples consist of varying proportions of R1 illite-smectite and R3 illite-smectite, kaolinite, pyrophyllite, and chlorite. The relative proportions of each type of illite-smectite (R1 and R3) in size separates of whole rock were modeled using NEWMOD (Table 4). The percent illite-smectite is plotted versus apparent K-Ar age in Figure 11 according to the procedures of Mossmann et al. (1992), Moss-

mann (1991), and Pevear (1992). The least-squares best fit line has intercepts of 175 Ma at 100 percent R3 illite-smectite and 98 Ma at 0 percent R3 illite-smectite and a Mesozoic and not Tertiary age is indicated for the youngest end member. However, the linear relationship is due largely to two of the six samples (O-5 and CC-2) and has a poor correlation (R^2 = 0.51). Without these two samples, the remaining 4 samples show ages of 159 to 167 Ma consistent with the 152 Ma fault mineralization age and the 147 Ma vein age within the gold orebody. In addition, all six samples contain >50 percent R3 illite-smectite, placing even greater uncertainty on the end-member ages and making the viability of this interpretation difficult to assess. Because of the poor correlation, simple linear mixing of R1 and R3 type clays of different discrete ages is unlikely and overprinting of thermal events is the best interpretation for the mixed ages in the Long Trail Shale.

Evaluation of mixed ages resulting from thermal resetting during multiple thermal events

Hydrothermal illite is abundant in the dated samples, but the multistage thermal history of Mercur requires that the possibility of diffusional loss of ^{40}Ar from illite be evaluated when interpreting the K-Ar data. Because temperatures of gold mineralization in sediment-hosted disseminated gold deposits are relatively low (150°–250°C) and near the closure temperature for the fine-grained illite used to date the hydrothermal activity, the time and temperature dependency of Ar diffusion within any previously existing illite plays an important part in determining the age relationships.

Diffusion in micas has been modeled as an infinite slab with Ar diffusion perpendicular to the cleavage planes and as a cylinder with diffusion radially parallel to cleavage. The geometry of the mica structure, along with the location and size of the Ar atom, suggests that diffusion occurs along the cleavage planes and that the cylindrical model is the best choice (Harrison et al., 1985; McDougall and Harrison, 1988). The effective diffusion radius in large particles of biotite or muscovite is about 150 μm (Robbins, 1972; Harrison et al., 1985; McDougall and Harrison, 1988). The maximum diffusion radius for mica particles smaller than 150 μm should then be equal to the particle radius. Particle thickness perpendicular to the cleavage planes was measured in this study using line broadening (Klug and Alexander, 1974) for five orders of X-ray diffraction peaks. Sample CS-13 has a mean
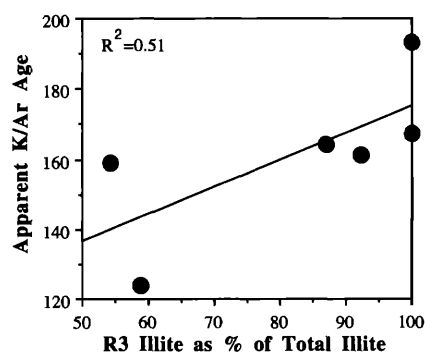

FIG. 11.   Apparent age and relative abundance of R3 illite from the Long Trail Shale.

thickness of 32 nm compared to a mean particle diameter of 650 nm (measured by photon correlation spectroscopy) showing that the illites are thin sheets and that the particle radius can be used as the diffusion radius in all samples from Mercur. The size range and particle size distribution are given in Figure 12.

Closure temperatures: The equation for calculating closure temperature in cooling systems given in Dodson (1973) is

$$T_c = \frac{\dfrac{E}{R}}{ln\left[\dfrac{ART_c^2\dfrac{D_0}{a^2}}{E\dfrac{dT}{dt}}\right]}. \tag{1}$$

The diffusion equations for various geometries given in Crank (1975), McDougall and Harrison (1988), and summarized in Dodson (1973) are

$$f = \sum_{n=1}^{\infty} \left[\frac{B}{a_n^2}\right] e^{[-a_n^2\,Dt/a^2]} \tag{2}$$

and

$$D = D_o e^{-E/RT}. \tag{3}$$

The symbols used in equations 1 to 3 are T_c = closure temperature, f = fraction Ar remaining, R = gas constant, E = activation energy = 40 kcal per mole (Robbins, 1972), A = geometric constant = 27 for a cylinder (Dodson, 1973), D_o = diffusion coefficient at infinite temperature = 3.02×10^{-4} cm^2/s (value from Robbins, 1972, and modified for cylinder model, McDougall and Harrison, 1988), D = diffusion coefficient, a = diffusion radius, dT/dt = cooling rate, $a_n = (n - \frac{1}{4})\pi$ for cylindrical geometry of radius a, B = 4 for cylindrical geometry, t = time.

The variation in closure temperature as a function of particle size and cooling rate calculated using equations 1 and 2
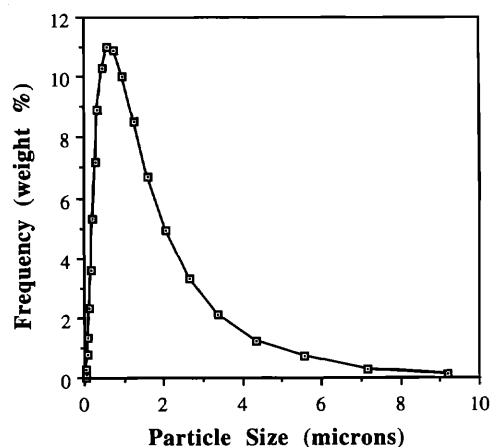

FIG. 12. Particle size distribution of clay from the Mercur mine as determined by photon correlation spectroscopy.
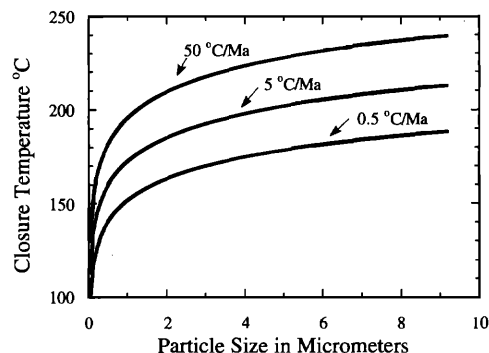

FIG. 13. Calculated closure temperatures for illite as a function of particle size and cooling rate.

is shown in Figure 13. A cooling rate of 50°C/Ma was used to approximate cooling after igneous intrusion. Cooling rates of 5 and 0.5°C/Ma were used to simulate cooling after burial metamorphism or a basin fluid flow event related to thrust faulting. Closure temperatures decrease with particle size, reflecting decreasing diffusion radius, and also decrease as the cooling rate is decreased, reflecting the time dependency of diffusion.

Closure temperatures were calculated for each particle size range that was dated (<2 or 0.03–0.3 μm) using equation 1 and the photon correlation spectroscopy-measured particle distribution within these size ranges as determined in representative sample CS-13. The closure temperature for each of these mixtures of particle sizes was estimated as the weighted-average of the closure temperature for the weight fraction of each particle size in the mixture. These closure temperatures are 143° to 179°C for <2-μm illite and 127° to 165°C for 0.03- to 0.3-μm illite.

If the age discordance among the Mercur mine samples results simply from exhumation and cooling, then the discordance should be small because all samples were taken from an area of about 3 km^2. Minor variation in age of a few million years might be expected as a result of variation in particle size distribution between the samples. However, the 130 Ma range in age of these samples requires unrealistic variation in particle size distribution from sample to sample.

Thermal resetting: Heating clay minerals to a temperature high enough to permit Ar diffusion from the clay structure will partially or completely reset the K-Ar systematics. Particle size influences thermal resetting in two related ways. First, fine clay particles completely reset at lower temperatures than coarse clay particles; and second, at temperatures below the temperature for complete resetting, the fine clays lose more Ar than the coarse clays. Both effects are due to the smaller diffusion radius of the finer particles. The observed age range can be modeled as a function of particle size effects during partial thermal resetting using the above equations and the results used to evaluate the effect of the known thermal events on the Mercur illite ages.

The Ar retention of clay-size fractions that were dated was calculated using equation 2, the activation energy for muscovite under hydrothermal conditions of Robbins (1972), and the particle size distribution measured by photon correlation spectroscopy . Argon diffusion curves were computed

for each of the dated particle size ranges, <2 and 0.03 to 0.3 μm, and for heating times of 2 and 10 Ma (Fig. 14). The shorter heating time of 2 Ma approximates the heating expected by shallowly emplaced igneous intrusions (Fig. 14A), and the longer heating time of 10 Ma approximates heating caused by a low-temperature metamorphic or basin fluid flow event (Fig. 14B). These diffusion curves are identical at the lower temperatures because the fine particles are present in both size fractions, but the curves diverge at higher temperatures because clay particles coarser than 0.3 μm in the <2-μm-size fraction retain argon at higher temperatures. At low temperatures neither size fraction loses Ar and both have the same age. At 150°C, the fine clay fraction has lost most of its Ar when heated for 10 Ma and its age is almost completely reset while the coarse clay retains 50 percent of its Ar. At 160°C the 0.03- to 0.3-μm-size fraction is completely reset. At 215°C the <2-μm-size fraction is completely reset. For the shorter heating time of 2 Ma these temperatures are 10° to 15°C higher (Fig. 14A). The Ar retention curves are compared with the empirical curve of Hunziker et al. (1986) in Figure 14B.

Temperatures of about 200°C should have totally reset the <2-μm-size fraction. Since burial to 7.5 km should have subjected these rocks to temperatures higher than this and since the pyrophyllite-bearing assemblage of the overlying Manning Canyon Shale indicates minimum temperatures of 260°C, there should be no detrital component remaining in the ages of the <2-μm-size fractions.
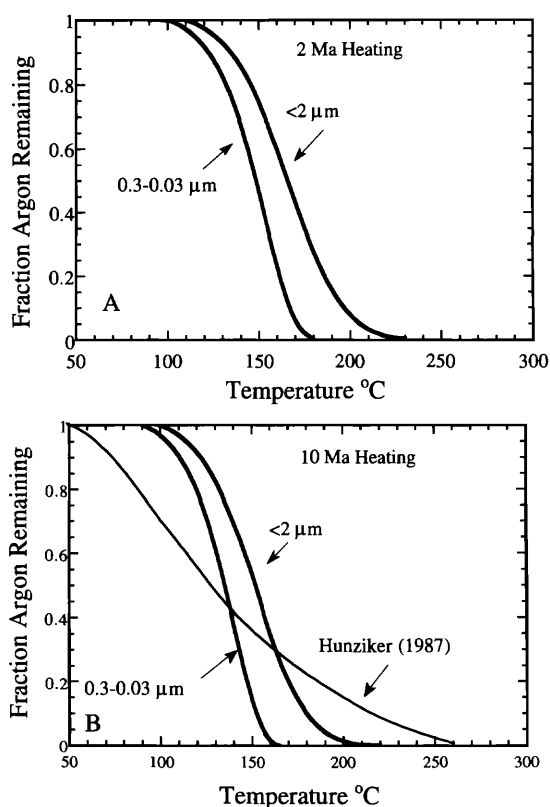

FIG. 14. Argon retention curves for dated clay fractions of <2 μm and 0.03 to 0.3 μm calculated using the diffusion equation in Dodson (1973). The empirical curve of Hunziker (1987) is given for comparison.

From this analysis, a temperature of about 230°C would have been required to reset the <2-μm-size fraction completely during heating caused by intrusion of the Eagle Hill Rhyolite. This temperature is much higher than the 50°C ambient temperature previously calculated to have occurred at 400 m from the rhyolite contact immediately after intrusion.

Interpretation

The progressive decrease in age as the Carrie Steele fault is approached is interpreted as mostly mixed ages representing increasing influence of hydrothermal fluids from the fault on the illite mineralogy of the rocks. Although the mineralogy is fairly uniform across the traverse, the progressive decrease in age as the fault is approached indicates that lesser amounts of older illite were destroyed and/or thermally reset by the hydrothermal fluids with increasing distance from the fault. The age of 152 Ma (0.03–0.3 μm) obtained from the north strand of this fault (sample CS-9) is consistent with several other dates of veins and altered Long Trail Shale (avg 160 Ma) obtained from within the Mercur district and an illite vein age of 147 Ma from the Sacramento pit (Wilson and Parry, 1990a; Table 4). Sample CS-9 is mineralized and strongly altered (30.3% kaolinite, 16.7 % illite, 1,800 ppm As, 200 ppm Sb, Table 3). As discussed in a previous section, the illite of sample CS-9 appears to be exclusively hydrothermal in origin. Illite in this sample has a strong felted fabric with obvious three-dimensional growth. Nothing in thin sections or hand specimens is suggestive of remnant sedimentary textures. The small age difference between the 0.03- to 0.3-μm and <2-μm-size fractions of sample CS-9 (152 and 167 Ma, respectively, with analytical uncertainty of ± 4 Ma) indicates that hydrothermal activity at the fault has destroyed or thermally reset the ages of nearly all older illitic minerals up to 2 μm in size and that an age of 152 Ma is the best estimate of the true age of the hydrothermal event causing argillic alteration on this fault. The presence of mixed ages is expected because of the multistage nature of the argillic alteration observed in thin sections from this traverse. The range in ages is surprising in that it suggests significant argillization of the limestone prior to the near 150 Ma event related to fluid movement on the fault.

Of the five ages obtained from the Mercur beds suite within the Mercur pit, the 149 and 138 Ma ages are generally consistent with a 147 Ma illite vein age obtained from the Sacramento pit (Wilson and Parry, 1990a) and the 152 Ma age of sample CS-9. The 98.4 Ma age of sample MB-1 (0.03–0.3 μm) may indicate resetting of illite ages by localized fluid movement on the Lulu fault. Ages less than 140 Ma were obtained from sample locations in the Long Trail Shale throughout the southern Oquirrh Mountains (Table 4) demonstrating the regional nature of this resetting event and that the Eagle Hill Rhyolite, with its limited thermal aureole, was probably not responsible for the resetting. Thermal resetting during the Sevier tectonic event at 100 ± 10 Ma is a more likely possibility. A 138 Ma age was also obtained for the 0.03- to 0.3-μm-size fraction of altered Long Trail Shale from the Daisy mine at West Dip (Table 4). This sample is from fault gouge on the West Mercur fault, a basin and range-type normal fault on the west side of the Oquirrh Mountains (Fig. 1). The very fine <0.03-μm-size fraction of this sample has

an age of 121 Ma, indicating little or no thermal resetting by Tertiary faulting or igneous activity.

The 222 (sample MM-1, <2-μm), 226 (sample MM-15, <2-μm), and 210 Ma (sample MM-15, 0.03- to 0.3-μm) ages obtained from the Magazine sandstone on both strands of the Lulu fault are consistent with the oldest ages from the Marion Hill pit. The oldest ages postdate maximum burial in the Oquirrh basin and are not significantly influenced by the presence of detrital illite. This conclusion is based on the following:

1. The deep burial of these sediments occurred during development of the Oquirrh basin. Data from shale studies in other regions indicate extensive recrystallization of shales to R3 illite-smectite upon burial to depths of 5 km and resetting of K-Ar ages (i.e., Aronson and Hower, 1976; Hower et al., 1976; Pollastro, 1990).

2. The ages are Late Triassic to earliest Jurassic and are significantly younger than the Mississippian stratigraphic age of the host rocks and are also younger than the time of maximum burial in the region estimated to have occurred at 260 Ma.

3. Within the Mercur district, size fractions as coarse as 10 μm have been extensively if not completely thermally reset within the Long Trail Shale (Wilson and Parry, 1990a).

4. Vein ages from hydrothermally altered Long Trail Shale are as old as 189 Ma and although the vein ages may be mixed ages, they cannot contain a detrital component.

5. Veins of the assemblage pyrophyllite + kaolinite + quartz in the overlying Manning Canyon Shale indicate that this unit has been subjected to minimum temperatures of 260°C, sufficiently high to have completely reset the <2-μm-size fraction.

6. Limestones of the CS series samples were originally massive limestones and contained little detrital illite, their current high illite and low calcite content must be postdepositional.

Similar Triassic to Jurassic ages have been obtained from the Barneys Canyon deposit in the northern Oquirrh Mountains in mineralized rocks of similar mineralogy (Presnell, 1992) which suggests taht this older illitization event may have occurred regionally. The somewhat younger ages obtained from the 0.03- to 0.3-μm-size fraction of samples CS-14 and MM-15 show that these oldest ages are at least slightly reset by the effects of younger hydrothermal activity and so the age of the older event is not well constrained.

The Mercur deposit has a complex thermal history that is still not well understood but appears to consist of an early event related to the Oquirrh basin, a hydrothermal event possibly related to gold at 140 to 160 Ma, and a late overprinting event which may have occurred during the Sevier orogeny. Tertiary igneous activity had very minor thermal effects and was not related to gold mineralization. Calling upon a large, buried intrusion for gold mineralization is not a valid hypothesis for Mercur. Gravity and magnetic data can be used to help establish this. Published gravity maps of northern Utah do not show gravity anomalies for any of the major igneous intrusions such as at Bingham or Alta (Cook and Berg, 1961). However, more detailed gravity surveys conducted by American Barrick within the district do not reveal

any gravity anomalies (Tracy Shier, chief mine geologist, pers. commun.). Published magnetic surveys (Mabey, 1992; Mabey et al., 1964; Stewart et al., 1977) do show magnetic anomalies for intrusions at Bingham, Stockton (11 km north of Mercur), and Tintic (30 mi south of Mercur), but not at Mercur. This is confirmed by more detailed aeromagnetic surveys done in the district by American Barrick (Tracy Shier, chief mine geologist, pers. commun.). In addition, a 2,062-ft drill hole (DOE 1) drilled by the U.S. Department of Energy at Mercur to test new deep drilling technology did not encounter any igneous rocks at depth and bottomed in unaltered Gardison Limestone. This hole was located in the Golden Gate area north and east of the Mercur pit and south and east of the Marion Hill pit (Fig. 3) and was collared at an elevation of 6,716 ft (Larry Stanger, mine geologist, pers. commun.).

Conclusions and Summary

Argillically altered limestones in the Mercur gold deposits contain illite, kaolinite, quartz, and pyrite. The illite is a 2M$_1$ polytype of an R3 interstratification of illite with <10% smectite. Ratios of illite to kaolinite are variable. The consistency of the illite + kaolinite + quartz alteration assemblage found in a range of host-rock types, altered limestone and sandstone within the gold deposits and the altered portions of the Long Trail Shale, along with the common heavy metal signature indicates that the alteration in all the units is related and the result of a large-scale hydrothermal event.

The K-Ar ages from within the gold deposits range from 98.4 to 226 Ma and the age data indicate a series of overprinted thermal and/or mass transfer events occurred at Mercur. The mixed nature of some of the age data and uncertainties in modeling mixed ages prevent a precise determination of the thermal history of the deposit. However, the data do suggest the following:

1. Thermal effects of the intrusion modeled using Cathles (1977) and Jaeger (1959) and spatial interpretation of the age data indicate that intrusion of the Eagle Hill Rhyolite at 30 Ma had very limited hydrothermal effects, had at most a limited role in creating the mixed ages, and was not related to the major stages of gold mineralization.

2. An age near 150 Ma is the best estimate of the true age of a hydrothermal event on the Carrie Steel fault. The progressive age distribution with distance from this fault demonstrates the existence of at least two thermal events which occurred in the rocks of this area prior to intrusion of the Tertiary Eagle Hill Rhyolite.

3. The older event indicated by the Triassic to mid-Jurassic ages occurred sometime after maximum burial during formation of the Oquirrh basin.

4. The data also suggest that a third regional thermal event occurred prior to the Tertiary which resulted in partial resetting of ages to between 98 and 140 Ma. This event may be related to the Sevier orogeny.

5. The best estimate of the age of gold mineralization is between 140 and 160 Ma which is the age of hydrothermal activity on one of the main structures controlling gold mineralization within the Mercur deposits, the age of vein illite within the Mercur deposits, and the age of widespread hydrothermal alteration of the Long Trail Shale throughout the

Mercur district. However, lack of petrographic evidence relating gold mineralization to illite precipitation and the multistage thermal history of the deposit prevents a precise determination of the age of gold mineralization at this time.

Acknowledgments

REFERENCES

Areliart, G.B., Foland, K.A., Naeser, C.W., and Kesler, S.E., 1993, $^{40}Ar/^{39}Ar$, K-Ar and fission track geochronology of sediment-hosted disseminated gold deposits at Post-Betze, Carlin trend, northeastern Nevada: ECONOMIC GEOLOGY, v. 88, p. 622–646.

Armstrong, R.L., 1968, Sevier orogenic belt in Nevada and Utah: Geological Society of America Bulletin, v. 79, p. 429–458.

Aronson, J.L., and Hower, J., 1976, Mechanism of burial metamorphism of argillaceous sediment: 2. Radiogenic argon evidence: Geological Society of America Bulletin, v. 87, p. 738–744.

Aronson, J.L., and Lee, M., 1986, K/Ar systematics of bentonite and shale in a contact metamorphic zone, Cerrillos, New Mexico: Clays and Clay Minerals, v. 34, p. 483–487.

Ashton, L.W., 1989, Geochemical exploration guidelines to disseminated gold deposits: Mining Engineering, March, p. 169–174.

Bakken, B.M., Hochella, M.F., Jr., Marshall, A.F., and Turner, A.M., 1989, High-resolution microscopy of gold in unoxidized ore from the Carlin mine, Nevada: ECONOMIC GEOLOGY, v. 84, p. 171–179.

Boles, J.R., and Franks, S.G., 1979, Clay diagenesis in Wilcox sandstones of southwest Texas: Implications of smectite diagenesis on sandstone cementation: Journal of Sedimentary Petrology, v. 49, p. 55–70.

Cathles, L.M., 1977, An analysis of the cooling of intrusions by ground-water convection which includes boiling: ECONOMIC GEOLOGY, v. 72, p. 804–826.

Clauer, N., and Chaudhuri, S., 1992, Indirect dating of sediment-hosted ore deposits: Promises and problems: Lecture Notes in Earth Sciences 43, p. 361–388.

Clauer, N., Savin, S.M., and Chaudhuri, S., 1992, Isotopic compositions of clay minerals as indicators of the timing and conditions of sedimentation and burial diagenesis: Lecture Notes in Earth Sciences 43, p. 239–286.

Cook, K.L., and Berg, J.W., 1961, Regional gravity survey along the central and southern Wasatch Front, Utah: U.S. Geological Survey Professional Paper 316–E, p. 75–89.

Crank, J., 1975, The mathematics of diffusion, second edition: Oxford, Clarendon Press, 414 p.

Dodson, M.H., 1973, Closure temperature in cooling geochronological and petrological systems: Contributions to Mineralogy and Petrology, v. 40, p. 259–274.

Ford, N.C., Jr., 1985, Light scattering apparatus *in* Pecora, R., ed., Dynamic light scattering: New York, Plenum Press, p. 7–58.

Gilluly, J., 1932, Geology and ore deposits of the Stockton and Fairfield quadrangles, Utah: U.S. Geological Survey Professional Paper 173, 171 p.

Harrison, T.M., Duncan, I., and McDougall, I., 1985, Diffusion of ^{40}Ar in

biotite: Temperature, pressure and compositional effects: Geochimica et Cosmochimica Acta, v. 49, p. 2461–2468.

Hemley, J.J., Montoya, J.W., Marinenko, J.W., and Luce, R.W., 1980, Equilibria in the system Al_2O_3-SiO_2-H_2O and some general implications for alteration-mineralization processes: ECONOMIC GEOLOGY v. 75, p. 210–228.

Hower, J., Eslinger, E.V., Hower, M.E., and Perry, E.A., 1976, Mechanism of burial metamorphism of argillaceous sediment: I. Mineralogical and chemical evidence: Geological Society of America Bulletin, v. 87, p. 725–737.

Hunziker, J.C., 1987, Radiogenic isotopes in very low-grade metamorphism, *in* Frey, M., ed., Low temperature metamorphism: London, Blackie, p. 201–226.

Hunziker, J.C., Frey, M., Clauer, N., Dallmeyer, R.D., Friedrichsen, H., Flehmig, W., Hochstrasser, K., Roggwiler, P., and Schwander, H., 1986, The evolution of illite to muscovite: Mineralogical and isotopic data from the Glarus Alps, Switzerland: Contributions to Mineralogy and Petrology, v. 92, p. 157–180.

Ilchik, R.P., 1990, Geology and geochemistry of the Vantage gold deposits, Alligator Ridge-Bald Mountain mining district, Nevada: ECONOMIC GEOLOGY, v. 85, p. 50–75.

Inoue, A., and Utada, M., 1983, Further investigations of a conversion series of dioctahedral mica/smectites in the Shinzan hydrothermal alteration area, northeast Japan: Clays and Clay Minerals, v. 31, p. 401–412.

Jaeger, J.C., 1959, Temperatures outside a cooling intrusive sheet: American Journal of Science, v. 257, p. 44–54.

Jewell, P.W., 1984, Chemical and thermal evolution of hydrothermal fluids, Mercur gold district, Tooele County, Utah: Unpublished M.Sc. thesis, Salt Lake City, University of Utah, 77 p.

Jewell, P.W., and Parry, W.T., 1987, Geology and hydrothermal alteration of the Mercur gold deposit, Utah: ECONOMIC GEOLOGY, v. 82, p. 1958–1966.

——1988, Geochemistry of the Mercur gold deposit (Utah, U.S.A): Chemical Geology, v. 69, p. 245–265.

Jordan, T.E., and Douglass, R.C., 1980, Paleogeography and structural development of the late Pennsylvanian to Early Permian Oquirrh basin, northwestern Utah: West-Central United States Paleogeography Symposium, 1st, Society of Economic Paleontologists and Mineralogists, Rocky Mountain Section, Denver Colorado, June 1980, p. 217–238.

Kisch, H.J., 1991, Illite crystallinity: Recommendations on sample preparation, X-ray diffraction settings and interlaboratory samples: Journal of Metamorphic Geology, v. 9, p. 665–670.

Klug, H.P., and Alexander, L.E., 1974, X-ray diffraction procedures, 2nd edition: New York, Wiley, 966 p.

Kornze, L.D., 1987, Geology of the Mercur gold mine, *in* Johnson, J.L., ed., Bulk mineable precious metal deposits of the western United States: Guidebook for field trips, Reno, Geological Society of Nevada, p. 381–389.

Kroko, C.T., 1992, Structural controls on gold distribution of the Mercur gold deposit, Mercur, Utah: Unpublished M.Sc. thesis, Salt Lake City, University of Utah, 150 p.

Kubler, 1967, La cristallinite de l'illite et les zones tout a fait superieures du metamorphisme en etages tectoniques: Etages Tectoniques Colloque, Neuchatel, Swisse, April 18–21, 1966, Proceedings.

Kuehn, C.A., and Rose, A.W., 1992, Geology and geochemistry of wall-rock alteration at the Carlin gold deposit, Nevada: ECONOMIC GEOLOGY, v. 87, p. 1697–1721.

Lebron, I., Suarez, D.L., Amrhein, C., and Strong, J.E., 1993, Size of mica domains and distribution of the adsorbed Na-Ca ions: Clays and Clay Minerals, v. 41, p. 380–388.

Lewis, D.W., 1984, Practical sedimentology: Stroudsburg, PA, Hutchinson Ross, 229 p.

Mabey, D.R., 1992, Subsurface geology along the Wasatch front: U.S. Geological Survey Professional Paper 1500-C, p. C1–C16.

Mabey, D.R., Crittenden, M.D., Jr., Morris, H.T., Roberts, R.V., and Tooker, E.W., 1964, Aeromagnetic and generalized geologic map of part of north-central Utah: U.S. Geological Survey Geophysical Investigations Map GP–422.

McDougall, I., and Harrison, T.M., 1988, Geochronology and thermochronology by the $^{40}Ar/^{39}Ar$ method: New York, Oxford University Press, 212 p.

Moore, D.M., and Reynolds, R.C., 1989, X-ray diffraction and the identification and analysis of clay minerals: New York, Oxford University Press, 332 p.

Moore, W.J., and McKee, E.H., 1983, Phanerozoic magmatism and mineral-

ization in the Tooele 1° by 2° quadrangle, Utah: Geological Society of America Memoir 157, p. 183–190.

Mossmann, J.R., 1991, K/Ar dating of authigenic illite-smectite clay material: Application to complex mixtures of mixed layer assemblages: Clay Minerals, v. 26, p. 189–198.

Mossmann, J.R., Clauer, N., and Liewig, N., 1992, Dating thermal anomalies in sedimentary basins: The diagenetic history of clay minerals in the Triassic sandstones of the Paris basin, France: Clay Minerals, v. 27, p. 211–226.

Parry, W.T., Ballantyne, J.M., and Bryant, N.L., 1980, Hydrothermal enthalpy and heat flow in the Roosevelt Hot Springs thermal area, Utah: Journal Geophysical Research, v. 85, p. 2556–2559.

Pevear, D.R., 1992, Illite age analysis, a new tool for basin thermal history analysis: International Symposium on Water-Rock Interaction, 7th, Park City, Utah, Proceedings, p. 1251–1254.

Presnell, R.D., 1992, Geology and geochemistry of the Barneys Canyon gold deposit, Salt Lake Co., Utah: Unpublished Ph.D. dissertation, Salt Lake City, University of Utah, 363 p.

Presnell, R.D., and Parry, W.T., 1992, Argillic alteration at the Barney's Canyon gold deposit: Utah Geological Survey Miscellaneous Publication 92–3, p. 313–318.

——in press, Evidence of Mesozoic deformation in the Oquirrh Mountains from the Barney's Canyon gold deposit: Geological Society of America Special Paper 299.

Presnell, R.D., Wilson, P.N., Kroko, C.T., and Parry, W.T., 1993, Constraints on ages of mineralization and deformation in the Oquirrh Mountains, Salt Lake Co., Utah [abs.]: Geological Society of America Abstracts with Programs, v. 25, no. 5, p. 135.

Pollastro, R.M., 1990, The illite-smectite geothermometer-Concepts, methodology, and application to basin history and hydrocarbon generation: Society of Economic Paleontologists and Mineralogists, Rocky Mountain Section, p. 1–18.

Reynolds, R.C., 1985, Description of program NEWMOD for the calculation of the one-dimensional X-ray diffraction patterns of mixed-layered clays: Hanover, New Hampshire, Dartmouth College, Department of Earth Sciences, 23 p.

Robbins, G.A., 1972, Radiogenic argon diffusion in muscovite under hydrothermal conditions: Unpublished M.Sc. thesis, Providence, Brown University, 88 p.

Srodon, J., 1984, X-ray powder diffraction identification of illitic materials: Clays and Clay Minerals, v. 32, p. 337–349.

Srodon, J., and Eberl, D.D., 1984, Illite: Reviews in Mineralogy, v. 3, p. 495–544.

Stanger, L.W., 1990, Geology and mineralization of the Lulu Graben, Barrick Mercur gold mine, Tooele, Utah: Society for Mining, Metallurgy, and Exploration Gold '90 Symposium, Salt Lake City, Utah, February 26-March 1, 1990, Proceedings, p. 11–19.

Stewart, J.H., Moore, W.J., and Zeitz, J., 1977, East-west patterns of Cenozoic igneous rocks, aeromagnetic anomolies, and mineral deposits, Nevada and Utah: Geological Society of America Bulletin, v. 88, p. 67–77.

Stock, R.S., and Ray, W.H., 1985, Interpretation of photon correlation spectroscopy data: A comparison of analysis methods: Journal of Polymer Science: Polymer Physics Edition, v. 23, p. 1393–1447.

Tafuri, W.J., 1987, Geology and geochemistry of the Mercur mining district, Tooele County, Utah: Unpublished Ph.D. dissertation, Salt Lake City, University of Utah, 180 p.

Watanabe, T., 1981, Identification of illite/montmorillonite interstratifications by X-ray powder diffraction: Mineralogical Society of Japan Journal, Special Issue 15, p. 32–41 (in Japanese).

Weiner, B.B., and Tscharnuter, W.W., 1987, Uses and abuses of photon correlation spectroscopy in particle sizing, *in* Provder, T., ed., Particle size distribution assessment and characterization: Washington, D.C., American Chemical Society, p. 48–61.

Wilson, P.N., 1992, Geochemistry and clay mineralogy of hydrothermally altered organic-rich shales, north-central Utah: Implications for a Mesozoic age of gold mineralization in the Mercur district: Unpublished Ph.D. dissertation, Salt Lake City, University of Utah, 269 p.

Wilson P.N., and Parry, W.T., 1989, Geochemical characteristics of hydrothermally altered black shales of the southern Oquirrh Mountains and relationships to Mercur-type gold deposits: Utah Geological and Mineral Survey Open-File Report 161, 68 p.

——1990a, Mesozoic hydrothermal alteration associated with gold mineralization in the Mercur district, Utah: Geology, v. 18, p. 866–868.

——1990b, Geochemistry of Mesozoic hydrothermal alteration of black shales associated with Mercur-type gold deposits: Society for Mining, Metallurgy, and Exploration Gold '90 Symposium, Salt Lake City, Utah, February 26-March 1, 1990, Proceedings, p. 167–174.

Wilson, P.N., Parry, W.T., and Nash, W.P., 1992, Characterization of hydrothermal tobelitic veins from black shale, Oquirrh Mountains, Utah: Clays and Clay Minerals, v. 40, p. 405–420.

Yonkee, W.A., Parry, W.T., Bruhn, R.L., and Cashman, P.H., 1989, Thermal models of thrust faulting: Constraints from fluid inclusion observations, Willard thrust sheet, Idaho-Utah-Wyoming Thrust Belt: Geological Society of America Bulletin, v. 101, p. 304–313.